









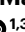

Profiling the proximal proteome of the activated μ -opioid receptor

Received: 27 July 2022

Accepted: 22 February 2024

Published online: 25 March 2024

 Check for updates

Benjamin J. Polacco ^{1,2,3,12}, Braden T. Lobingier^{4,12}, Emily E. Blythe ^{1,3,5}, Nohely Abreu ⁶, Prachi Khare^{1,2,3}, Matthew K. Howard ^{7,8,9}, Alberto J. Gonzalez-Hernandez ⁶, Jiewei Xu^{1,2,3}, Qiongyu Li^{1,2,3}, Brandon Novy⁴, Zun Zar Chi Naing^{1,2,3}, Brian K. Shoichet ^{1,8}, Willow Coyote-Maestas^{1,7,10}, Joshua Levitz ⁶, Nevan J. Krogan ^{1,2,3}, Mark Von Zastrow ^{1,3,5} ✉ & Ruth Hüttenhain ^{1,2,3,11} ✉

The μ -opioid receptor (μ OR) represents an important target of therapeutic and abused drugs. So far, most understanding of μ OR activity has focused on a subset of known signal transducers and regulatory molecules. Yet μ OR signaling is coordinated by additional proteins in the interaction network of the activated receptor, which have largely remained invisible given the lack of technologies to interrogate these networks systematically. Here we describe a proteomics and computational approach to map the proximal proteome of the activated μ OR and to extract subcellular location, trafficking and functional partners of G-protein-coupled receptor (GPCR) activity. We demonstrate that distinct opioid agonists exert differences in the μ OR proximal proteome mediated by endocytosis and endosomal sorting. Moreover, we identify two new μ OR network components, EYA4 and KCTD12, which are recruited on the basis of receptor-triggered G-protein activation and might form a previously unrecognized buffering system for G-protein activity broadly modulating cellular GPCR signaling.

The μ OR mediates the effects of endogenously produced peptide neuromodulators and represents the main pharmacological target for a large class of exogenously administered nonpeptide agonists, which are clinically used for treating pain^{1,2}. The μ OR is a member of the large GPCR superfamily, which operates essentially by allostery, coupling agonist-induced effects on receptor conformation to the binding of cytoplasmic proteins, which mediate downstream signaling and regulation³. While the interactions of the μ OR with known proteins, such as G proteins, GPCR kinases (GRKs) and arrestins, are well characterized, it is clear that

signaling through the μ OR is coordinated by additional proteins in the proximal receptor interaction network, operating as signal transducers, organizers or regulators^{4,5}. Moreover, little is known of how the interactions engaged by the receptor are organized and regulated in time and space in intact cells. The discovery of new μ OR proximal interactors and their cellular organization have largely remained invisible given the lack of technologies to interrogate these networks systematically.

Recently, we and others established GPCR-APEX, a proximity labeling method based on fusing an engineered ascorbic acid peroxidase

¹Quantitative Biosciences Institute (QBI), University of California, San Francisco, CA, USA. ²J. David Gladstone Institutes, San Francisco, CA, USA.

³Department of Cellular and Molecular Pharmacology, University of California, San Francisco, CA, USA. ⁴Department of Chemical Physiology and Biochemistry, Oregon Health and Sciences University, Portland, OR, USA. ⁵Department of Psychiatry and Behavioral Sciences, University of California San Francisco, San Francisco, CA, USA. ⁶Department of Biochemistry, Weill Cornell Medicine, New York, NY, USA. ⁷Department of Bioengineering and Therapeutic Sciences, University of California San Francisco, San Francisco, CA, USA. ⁸Department of Pharmaceutical Chemistry, University of California San Francisco, San Francisco, CA, USA. ⁹TETRAD Graduate Program, University of California San Francisco, San Francisco, CA, USA. ¹⁰Chan Zuckerberg Biohub, San Francisco, CA, USA. ¹¹Department of Molecular and Cellular Physiology, Stanford University, Stanford, CA, USA. ¹²These authors contributed equally: Benjamin J. Polacco, Braden T. Lobingier. ✉ e-mail: mark.vonzastrow@ucsf.edu; ruthh@stanford.edu

(APEX2) to the receptor^{6,7}, taking snapshots of the proximal receptor proteome with minute resolution and analyzing the receptor-proximal labeling profile using quantitative mass spectrometry (MS)^{8,9}. We previously demonstrated that GPCR-APEX can simultaneously capture the proximal protein interaction networks and the cellular location of activated receptors in a systematic manner through the quantification of thousands of proteins that are biotinylated proximal to the receptor. However, a major limitation to the application of GPCR-APEX has been to resolve information about changes in the local interaction network, obtained from the complex proteomic datasets, from changes in the subcellular location of receptors⁸.

Here we describe a new computational framework that: (1) models time-dependent subcellular location of the activated receptor by utilizing a system of spatially specific APEX2 references; and (2) quantitatively deconvolutes the effect of receptor location and proximal interactors in the proximity labeling data. We apply this framework to the μ OR after activation with three chemically diverse agonists—the opioid peptide agonist DAMGO, the opiate alkaloid partial agonist morphine and the chemically distinct ‘biased’ partial agonist PZM21 (ref. 10). We reveal substantially different effects on the μ OR proximal protein environment across the agonists. We establish that most of these differences are driven by agonist-selective receptor trafficking in the endocytic pathway and that these, in turn, are associated with agonist-selective differences in μ OR recruitment of endogenous β -arrestins. Moreover, we show that GPCR-APEX also has the ability to discover new μ OR proximal network components modulating receptor trafficking and signaling. VPS35 and COMMD3, two proteins primarily labeled in the proximity of the DAMGO-activated μ OR, influence receptor distribution between cell surface and intracellular compartments. Furthermore, we found that EYA4 and KCTD12, which are recruited into the μ OR proximal network by all agonists tested and are dependent on G_i activity, have significant but distinct effects on μ OR signaling by interacting directly with the G-protein subunits rather than the receptor itself.

Results

Subcellular location drives μ OR proximal proteome changes

We utilized APEX-based proximity biotin labeling and quantitative MS to investigate how activation of the μ OR controls the proximal proteome environment in an unbiased manner⁸. To map proximal proteome changes of the μ OR, we chose three agonists, DAMGO, morphine and PZM21 (ref. 10), which represent distinct chemistries and different efficacies and cellular responses to receptor activation. DAMGO is a peptide full agonist causing strong activation of both G-protein and β -arrestin pathways¹¹, while morphine, a naturally occurring alkaloid, acts as a partial agonist for both pathways^{11,12}. PZM21, a synthetic μ OR agonist unrelated to classic morphinans, exhibits partial agonism for G-protein activation and negligible activation of the β -arrestin pathway¹⁰. After stably expressing the μ OR-APEX2 fusion construct in HEK293 cells, we confirmed receptor functionality with regard to signaling, internalization and recycling (Extended Data Fig. 1a–c). For proximity labeling we pretreated cells with biotin-phenol followed by μ OR activation using all ligands at a concentration of 10 μ M over a 60-min time course (Fig. 1a). We used saturating concentrations for all ligands to ensure full receptor occupancy and therefore maximal receptor activation and biotinylation of proximal proteins. At selected time points, we initiated proximal biotin labeling by addition of hydrogen peroxide (H₂O₂) for 30 s, followed by cell lysis and enrichment of biotinylated proteins. Relative abundance changes of biotin-labeled proteins after agonist stimulation were quantified using a combination of unbiased and targeted proteomics approaches.

We leveraged the hundreds of proteins in our proximity labeling data to determine how μ OR trafficking, and thus the receptor's subcellular location, changed in a time- and agonist-dependent manner (Fig. 1b). To this end, we performed a statistical analysis determining

proteins with significant changes in biotin labeling over the time course. For each observed protein and ligand, we scored changes in biotin labeling by fitting the time course with a polynomial curve and performed an *F*-test comparing it against a model with no time term. A single significance score for each protein and ligand was calculated summarizing the confidence, strength and direction of the biotin labeling changes by combining the maximum fold change over the time course as a measure of strength and direction with the *P* value as a measure for confidence (Methods and Supplementary Table 1). Following hierarchical clustering of the significant proteins on the basis of their significance score across the three ligands, we performed gene ontology (GO) enrichment analysis for each cluster.

This unbiased view of the proximal protein environment of the activated μ OR indicated that: (1) most changes in biotin-labeled proteins are evoked by receptor endocytosis and trafficking; and (2) the three ligands differ strongly in their capacity to induce endocytosis and trafficking (Fig. 1b and Extended Data Fig. 1d). Targeted proteomics of selected localization markers for plasma membrane, early endosome and late endosome/lysosome confirmed these findings (Supplementary Table 2). DAMGO shifted the μ OR distribution from the plasma membrane to endosomes and lysosome, while morphine resulted in less endocytosis and, astonishingly, PZM21 led to no detectable changes in μ OR localization at the plasma membrane at all, something that is perhaps consistent with the functional selectivity for which it was developed¹⁰ (Fig. 1c). Fluorescent imaging confirmed colocalization of the DAMGO-activated μ OR with the early endosomal marker EEA1, but little and negligible colocalization upon activation with morphine and PZM21, respectively (Extended Data Fig. 1e). Together these data underscore how structurally distinct ligands can strongly influence the subcellular location of a receptor, and highlight the need for a systematic approach to identify the location-specific proximal proteome(s).

Computational framework to model receptor trafficking

To quantitatively model μ OR location across subcellular compartments we used spatially specific APEX2 references, that is, APEX2 constructs that are localized to selected subcellular compartments⁸. Previously, we relied on independent trafficking assays to determine the combination of reference conditions to best reflect the spatial position of a GPCR at a given time point after agonist addition. Here, we develop a computational framework to extract this information directly from the proximity labeling datasets, eliminating the need for prior knowledge of receptor trafficking. This framework quantitatively determines the localization of the spatial controls for each ligand and time point, facilitating the deconvolution of complex proteomic profiles captured by μ OR-APEX2, which can traffic to different compartments over longer timescales. The goal of this analysis is to discern: (1) spatial bystanders, that is, location-specific proteins in the local environment of the receptor that do not physically interact or directly participate in its function; and (2) proximal protein networks that can regulate receptor signaling and trafficking.

First, relevant spatial references for the plasma membrane (PM-APEX2), early endosome (Endo-APEX2) and lysosome (Lyso-APEX2) (Fig. 2a) were selected and validated to localize to and biotinylate proteins at the respective subcellular compartment (Extended Data Fig. 2a,b). Spatial reference samples were collected and analyzed alongside the μ OR proximity labeling samples. We then determined indicative proteins for subcellular locations by pairwise comparison of the biotin labeling data from the three spatial references using statistical models implemented in MSstats¹³. Proteins were considered location indicators if they: (1) showed a *P* value below 0.005 and a log₂ (fold change) (log₂FC) higher than 1.0 for at least one of the comparisons; and (2) were consistently quantified across all replicates above a defined intensity threshold (Fig. 2b and Supplementary Table 3). Next, we used these indicator proteins to estimate the ligand-dependent fraction of the μ OR at a given cellular location over the time course. Specifically,

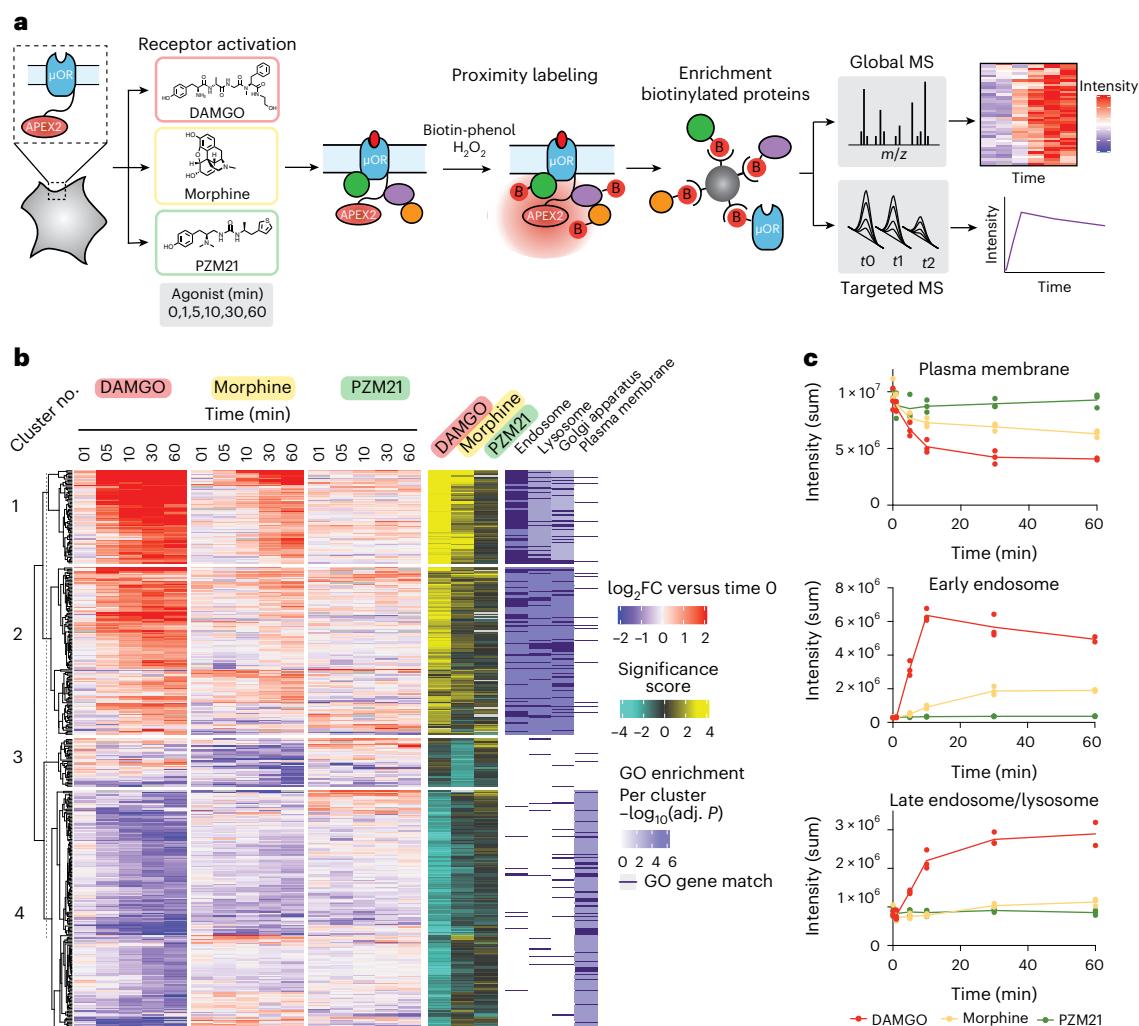


Fig. 1 | Ligand-dependent proximal proteome changes of the μ OR are driven by cellular location. **a**, Experimental design of the study. The μ OR-APEX2 construct was stably expressed in HEK cells. The receptor was activated with 10 μ M DAMGO, morphine and PZM21 over a time course of 60 min. Cells were pretreated with biotin-phenol for 30 min and biotinylation was initiated by the addition of H_2O_2 for 30 s at indicated time points after agonist treatment. Following cell lysis, biotinylated proteins were enriched using streptavidin and subsequently quantified using global and targeted MS approaches. **b**, Global agonist-dependent changes in proximal proteome of the μ OR. Heat map visualizing all proteins with a significant ($P < 0.01$, \log_2 (fold change) > 1) change in biotin labeling for at least one of the ligands across the time course.

The heat map was clustered according to the significance score, calculated as a combination of the $-\log_{10}$ (P value) and \log_2 (fold change). Gene ontology enrichment analysis was performed for individual clusters and significant gene ontology terms for the individual clusters and significant genes are indicated in dark purple. Data from three biological replicates are presented as mean. **c**, Targeted proteomics analysis of agonist-dependent biotinylation by μ OR-APEX2 of selected localization markers for plasma membrane (top), early endosome (middle) and late endosome/lysosome (bottom). Data from three biological replicates for DAMGO (red), morphine (yellow) and PZM21 (green) are presented. adj., adjusted.

we calculated location coefficients for each ligand, time point and biological replicate by solving a linear model based on the protein intensities of the location indicators across the spatial references and across the μ OR-APEX2 samples (Fig. 2c). The model-based cellular location coefficients for the receptor accurately recapitulated the relative locations determined experimentally by targeted proteomics (Fig. 1c) and fluorescent imaging (Extended Data Fig. 1e) and were consistent with previous studies investigating ligand-dependent μ OR trafficking¹⁴. Taken together, these results suggest that our computational framework is effective in modeling receptor trafficking.

We then leveraged the model-based coefficients to deconvolve the two time-dependent profiles of spatial bystanders and proximal protein interaction networks. To this end, we calculated expected intensities for all proteins in the μ OR-APEX2 dataset on the basis of the cellular location changes of the receptor. We combined the location coefficients for each ligand, time point and biological replicate

and the intensities of all proteins quantified across the PM, Endo and Lyso-APEX2 spatial references (Fig. 2d and Extended Data Fig. 3). Finally, assuming that observed protein intensities are a combination of both μ OR proximal interaction networks and spatial bystanders, we detrended the observed protein intensities for each ligand, time point and replicate combination with the spatially expected protein intensities. In brief, a protein's expected intensity, based on spatial references and ligand/time-specific coefficients, was subtracted from its observed intensity to produce a detrended intensity (Supplementary Table 4). For instance, detrending effectively accounted for the increase in biotin labeling observed for EEAL, a spatial bystander of the μ OR at the early endosome and therefore an indicator for receptor trafficking, after activation of the receptor with DAMGO and morphine (Fig. 2e, left panel). However, detrending did not affect the agonist-dependent temporal profiles for ARRB2 (Fig. 2e, right panel), a protein recruited to μ OR upon activation and known to regulate receptor trafficking

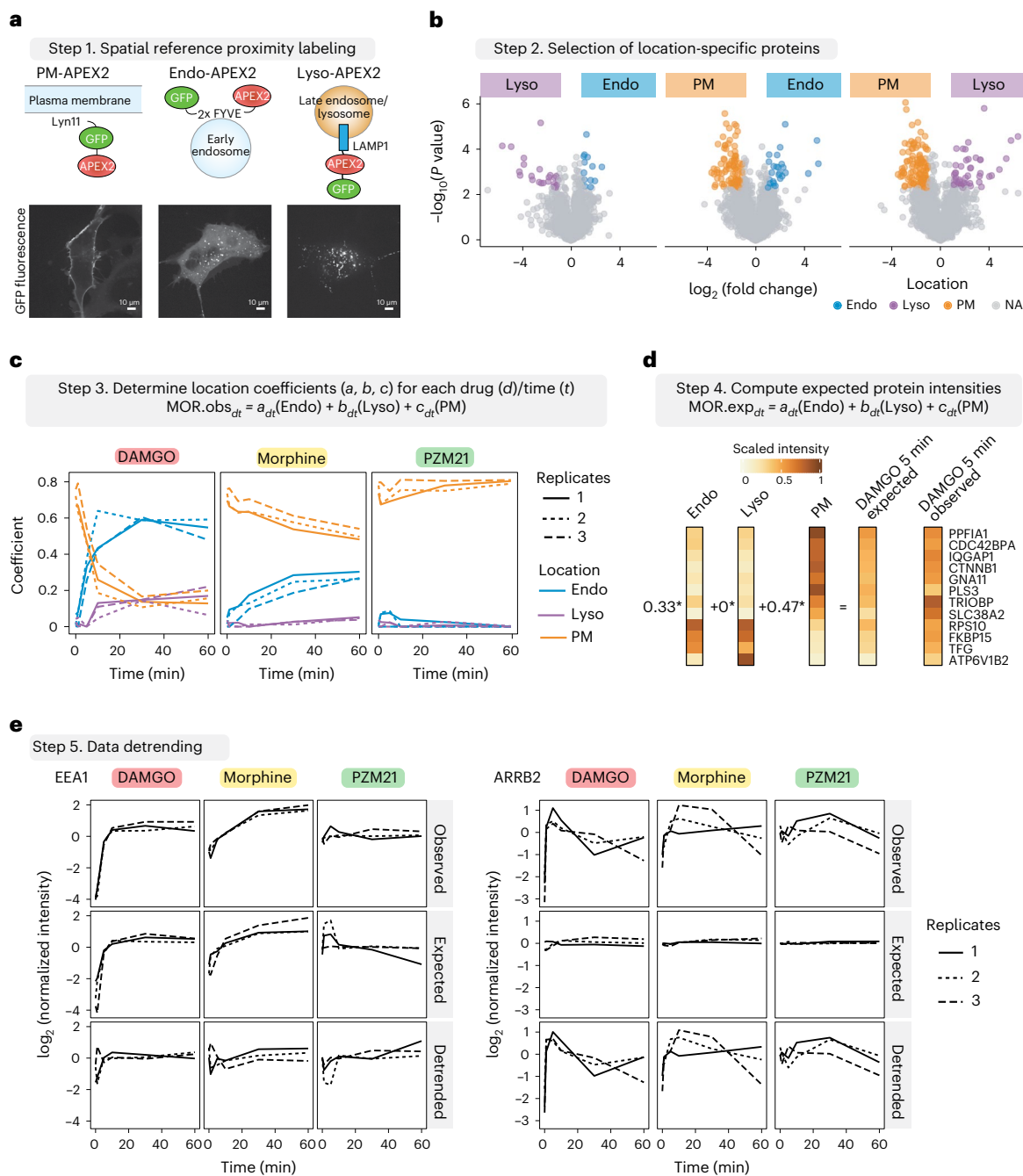


Fig. 2 | Computational framework to model ligand and time-dependent receptor location and deconvoluting receptor location from local interaction network. **a**, Step 1. Proximity labeling of spatial references. APEX2-tagged constructs targeting APEX2 to the plasma membrane (PM-APEX2), early endosome (Endo-APEX2) or lysosome (Lyso-APEX2) (top). Micrographs of PM-APEX2, Endo-APEX2 and Cyto-APEX2 using live-cell confocal imaging (bottom). Scale bars, 10 μ m. **b**, Step 2. Selection of location-specific indicator proteins. Volcano plots depicting pairwise comparison of spatial references. Proteins were required to: (1) have a P value below 0.005 and a $\log_2\text{FC} > 1.0$ for at least one of the comparisons; and (2) be consistently quantified across all replicates with an intensity greater than the 50th percentile to be selected as location-specific proteins for plasma membrane (PM, orange), endosome (Endo, blue) and lysosome (Lyso, purple). Data from three biological replicates are presented. **c**, Step 3. Determination of location-specific

coefficients. Intensities of location-specific indicator proteins are utilized to calculate coefficients for each location and ligand on the basis of the linear model. Data from three biological replicates are presented. **d**, Step 4. Computing expected protein intensities. Expected intensities for all proteins quantified in the dataset are calculated on the basis of location-specific coefficients and protein intensities measured for the spatial references. A subset of the data is shown as an example. **e**, Step 5. Data detrending. Data detrending process to dissect localization-specific effect from effect of interaction with the receptor is exemplified for EEA1 (spatial bystander) and ARRB2 (known μ OR interactor). Three different temporal profiles are depicted for each protein, ligand and replicate: the initial observed intensities (top), the expected intensities based on the location-specific references (middle) and the intensities after detrending (bottom). Data from three biological replicates are presented. exp, expected; MOR, μ OR; obs, observed.

and signaling, or members of the AP2 complex (Extended Data Fig. 4), which bind the receptor/ β -arrestin complexes in clathrin-coated pits.

The computational framework enables modeling of receptor trafficking directly from proximity labeling data, minimizing the need

for independent measurements with complementary methods. Thus, modeling requires minimal knowledge of the receptor trafficking itinerary and its kinetics, but instead predicts it on the basis of the quantitative measurement of multiple proteins. Additionally, the

framework can subtract location-specific trends from the μ OR-APEX2 dataset, enriching functionally relevant proteins in the receptor's proximal interaction network, such as ARRB2 and AP2 complex members. Importantly, this approach, demonstrated here for the μ OR, is readily applicable to other GPCRs and, more generally, signaling receptors across biology.

Ligand-dependent proximal interactions of the activated μ OR

After detrending the proximity labeling dataset to account for spatial bystander proteins, we sought to identify novel proteins in the proximal interaction network of μ OR and compare across the three ligands. To this end, we determined proteins with significant changes in biotinylation by fitting the time course with a polynomial curve and performing an *F*-test to compare it against a model with no time term on the detrended protein intensities. Proteins with significant changes in biotinylation ($\log_2FC > 1$ and *P* value < 0.001) before and after data detrending for at least one ligand were considered part of the proximal interaction network of the μ OR (47 proteins) and were clustered on the basis of their significance score across the ligands (Fig. 3a and Supplementary Table 5). We applied a more stringent significance cutoff for the detrended dataset to focus on proteins with higher confidence.

DAMGO evoked most significant changes in the proximal interaction network, enriched for proteins regulating endocytosis and trafficking, while PZM21 showed only minimal changes (Fig. 3a,b). Rather than engaging entirely different proteins, our data suggest that morphine- and PZM21-mediated activation of the μ OR result in a subset of the proximal protein network compared to DAMGO, probably differing in interactors involved in receptor endocytosis and trafficking (Fig. 3b). For example, ARRB2 showed a strong biotin labeling change upon activation of the μ OR with DAMGO, less with morphine and no visible change in biotin labeling with PZM21, consistent with its original design¹⁰ (Fig. 3c). Notably, consistent with previous findings, ligand-dependent changes in ARRB2 biotin labeling correlated with the degree of μ OR endocytosis, as predicted by the location coefficients (Fig. 3d and Extended Data Fig. 5)¹⁴.

To ask whether the μ OR proximal protein network derived from HEK293 cells can be recapitulated in cells expressing the receptor endogenously, we next performed a proximity labeling experiment for the DAMGO-activated μ OR in the SH-SY5Y neuroblastoma cell line. Most proteins (40 of 42) of the DAMGO-evoked proximal proteome network components identified in HEK293 cells were also captured in SH-SY5Y cells, with similar kinetics observed between the two systems (Extended Data Fig. 6 and Supplementary Table 6). Furthermore, while WASHC4 or RUFY2 did not show a DAMGO-dependent response in SH-SY5Y cells, we observed a response for related family members WASH2C and RUFY1, respectively. One exception is the hit identified in HEK293 cells, COMMD3, which showed a distinct pattern in SH-SY5Y cells. Thus, these data demonstrate that most of the proteins we identified in HEK293 cells were also found in SH-SY5Y cells, suggesting a general conservation of proteins regulating GPCR signaling and trafficking across different cell types.

COMMD3 and VPS35 impact μ OR subcellular distribution

Since the proximal interaction network of the DAMGO-activated μ OR was enriched for proteins related to endocytosis and endosomal trafficking, we wanted to explore influence on the μ OR subcellular distribution. First, we devised an assay to measure cellular receptor distribution using N-terminal tagging of the μ OR with a HaloTag (Fig. 4a). Sequential labeling of the HaloTag with an impermeable (JF635i) Halo dye, followed by a membrane-permeable (JF525) Halo dye, enabled differential labeling of the cell surface and intracellular receptor pools (Fig. 4b).

We then selected nine proximal μ OR network components for CRISPR knockout (KO) to evaluate their role in μ OR internalization, trafficking or recycling. Criteria for selection included: (1) proteins with changes in proximity labeling primarily for DAMGO-activated receptor;

(2) proteins with a proximity labeling profile that is little affected by data detrending; and (3) previous evidence of the protein function in trafficking. ARRB2, expected to decrease receptor internalization, was selected as a positive control, while a nontargeting control (NTC) was included as negative control. Briefly, for each target gene and the NTCs, three guide RNAs (gRNA) were individually complexed with Cas9 and electroporated into Halo- μ OR HEK293T cells. Using VPS35 as an example, we demonstrated high knockout efficiency (Fig. 4c).

The effects of gene knockout on μ OR cellular distribution were assessed before and after receptor activation with DAMGO for 30 min by sequential labeling with impermeable and membrane-permeable fluorescent Halo dyes and subsequent flow cytometry analysis (Fig. 4a). For each gRNA and time point, we calculated a surface-to-intracellular receptor ratio and assessed DAMGO-dependent receptor redistribution by comparing the surface-to-intracellular receptor ratios before and after μ OR activation (Fig. 4d). ARRB2 knockout significantly reduced receptor internalization compared to the NTC (Fig. 4d), as expected. Intriguingly, unlike ARRB2, VPS35 and COMMD3 knockout decreased the surface-to-intracellular receptor ratio with and without μ OR activation (Fig. 4e). This suggests that VPS35 and COMMD3, like ARRB2, are recruited into the μ OR interaction network selectively by DAMGO, but they produce a distinct functional effect on μ OR trafficking. Together, these findings highlight the ability of our methodology to identify novel agonist-specific network components with different effects relative to previously known network components.

EYA4 and KCTD12 are G-protein-dependent proteins near the μ OR

Despite ligand-dependent differences in the μ OR proximal interaction network, we discovered two proteins, EYA4 and KCTD12, exhibiting increased biotin labeling upon receptor activation with all ligands (Fig. 5a). While EYA4 displayed a consistent profile across ligands, the temporal profile for KCTD12 varied for the DAMGO-activated μ OR compared to PZM21 and morphine activation. EYA4 encodes a protein that acts as a transcriptional co-activator when tethered to DNA through interaction with the SIX family of homeodomain proteins¹⁵, but also possesses phosphothreonine and phosphotyrosine phosphatase activity. Previous studies have shown that EYA2, another member of the Eyes absent (EYA) protein family, can interact and colocalize with constitutively active $G\alpha_i$ proteins^{16,17} mediating an attenuation of cAMP inhibition¹⁷. KCTD12 encodes a protein that forms an auxiliary subunit for the GABA_B receptor regulating the rise time and duration of G-protein-coupled inwardly rectifying potassium channels (GIRKs)^{18,19} by competing with GIRK binding to the released $G\beta\gamma$ subunit and thus rapidly stripping $G\beta\gamma$ subunits from the activated channel, resulting in channel closure²⁰.

On the basis of this prior knowledge, and given their labeling upon activation of μ OR with all ligands, including those that stimulate negligible trafficking, we hypothesized that both proteins might regulate G-protein signaling downstream of the μ OR. Indeed, a proximity labeling experiment of the plasma membrane (PM-APEX2) upon activation of the μ OR with DAMGO in the presence and absence of the $G\alpha_i$ inhibitor pertussis toxin (PTX) validated the recruitment of KCTD12 and EYA4 to the plasma membrane in a μ OR and G_i -dependent manner (Fig. 5a,b). Interestingly, PTX treatment in the absence of μ OR activation (time point, 0 min) decreased biotin labeling of EYA4 at the plasma membrane significantly ($\log_2FC = -1.0$, *P* value = 2×10^{-8} ; Fig. 5b), suggesting some pre-existing binding of EYA4 before μ OR activation. Indeed, affinity purifications of EYA4 revealed its interaction with $G\alpha_i$ proteins at basal levels in addition to known interactors, including SIX proteins (Fig. 5c). Moreover, we found that the A633R SIX-binding mutation interfered with interaction of both $G\alpha_i$ and SIX proteins, while the D375N phosphatase-dead mutant did not alter the interactions (Fig. 5c). Finally, APEX2-based proximity labeling for EYA4 indicated a G_i -dependent increase in labeling of plasma membrane

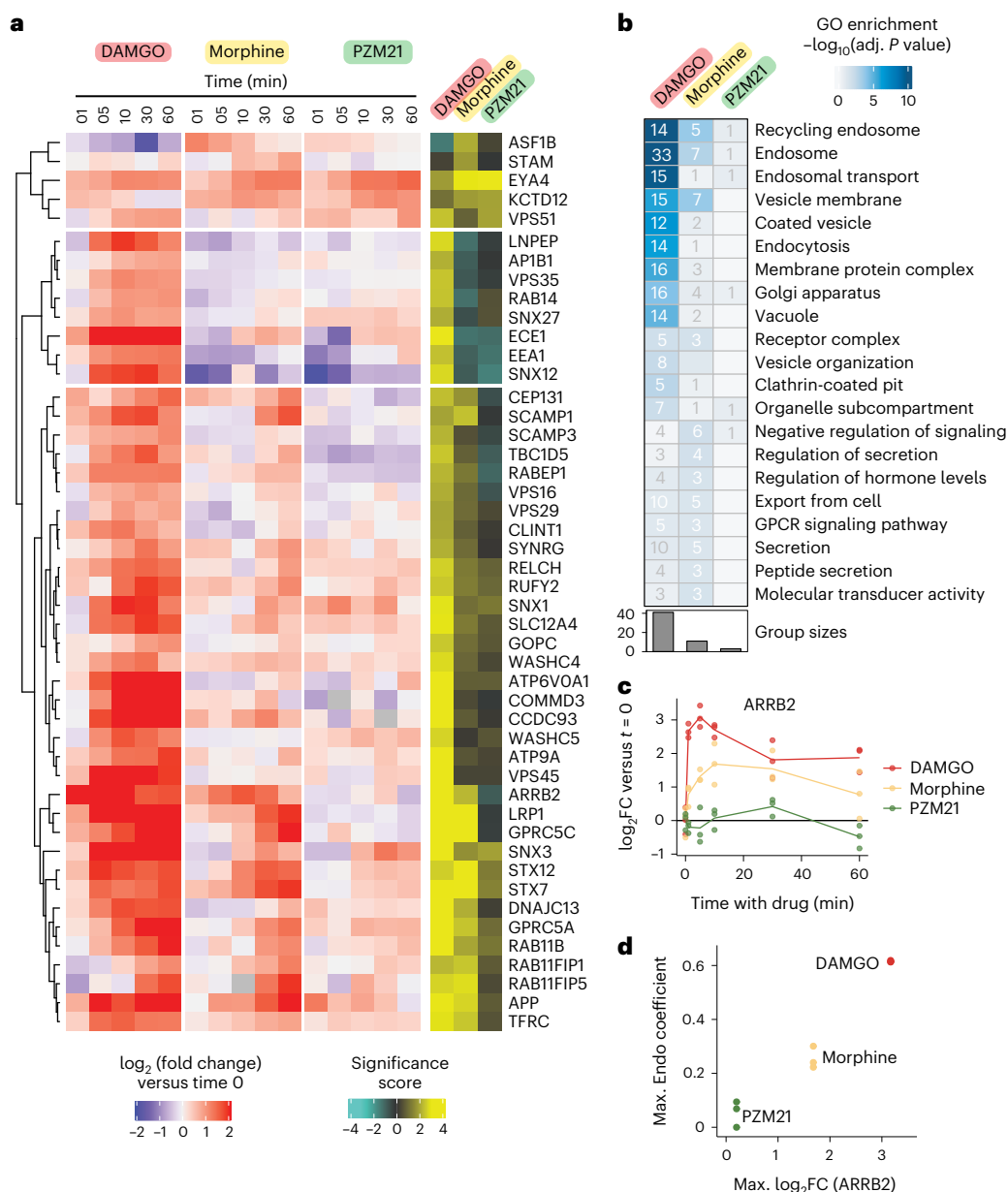


Fig. 3 | Ligand-dependent proximal interaction network of μ OR differs in interactors involved in receptor endocytosis and trafficking. **a**, Ligand-dependent proximal protein interaction networks of μ OR. All proteins are visualized in the heat map that showed a significant difference in biotin labeling (\log_2 FC > 1 and P value < 0.001) before and after location-specific detrending for at least one of the ligands across the time course. The heat map was clustered according to the significance score calculated as a combination of the $-\log_{10}$ (P value) and \log_2 FC. Data from three biological replicates are presented as mean. **b**, GO enrichment analysis for proteins of the ligand-dependent μ OR proximal interaction networks. The heat map shows all significantly enriched

GO terms (adjusted P value < 0.05) among the proteins present in the proximal interaction network of the μ OR including the number of proteins that match the GO terms. **c**, Temporal profile for ARRB2. Line charts represent the \log_2 FC over the time course of receptor activation with DAMGO (red), morphine (yellow) and PZM21 (green) after data detrending. Data from three biological replicates are presented as individual points and as mean in lines. **d**, Correlation between the maximum location coefficient calculated for the endosome (Endo) and the maximum ARRB2 \log_2 FC over the time course of μ OR activation with DAMGO (red), morphine (yellow) and PZM21 (green).

and a decrease in labeling of nuclear proteins (Fig. 5d,e and Extended Data Fig. 7).

Taken together, our data suggest that EYA4 and KCTD12 are recruited in the proximity of the μ OR in a receptor- and G_i activity-dependent manner, potentially regulating μ OR signaling through G proteins. However, on the basis of the previous finding that the GABA $_B$ seems to be the only direct receptor target of KCTD12 (ref. 19) and our experimental data for EYA4, we hypothesize that these regulatory proteins do not engage the receptor itself, but rather interact with the $G\beta\gamma$ and $G\alpha_i$ subunits, respectively, which are released by

dissociation of the heterotrimeric G protein upon μ OR activation. Thus, our data demonstrate that a strength of proximity labeling is the ability not only to identify direct μ OR interactors, but also to capture parts of the proximal proteome acting downstream of the activated receptor.

EYA4 and KCTD12 modulate signaling through G proteins

Our findings indicate that EYA4 interacts with $G\alpha_i$ subunits (Fig. 5c), while KCTD12 binds to $G\beta\gamma$ subcomplexes, as previously established^{18,19}. Thus, we focused on cellular G-protein signaling for initial functional assessment, assaying signaling through cytoplasmic cAMP production.

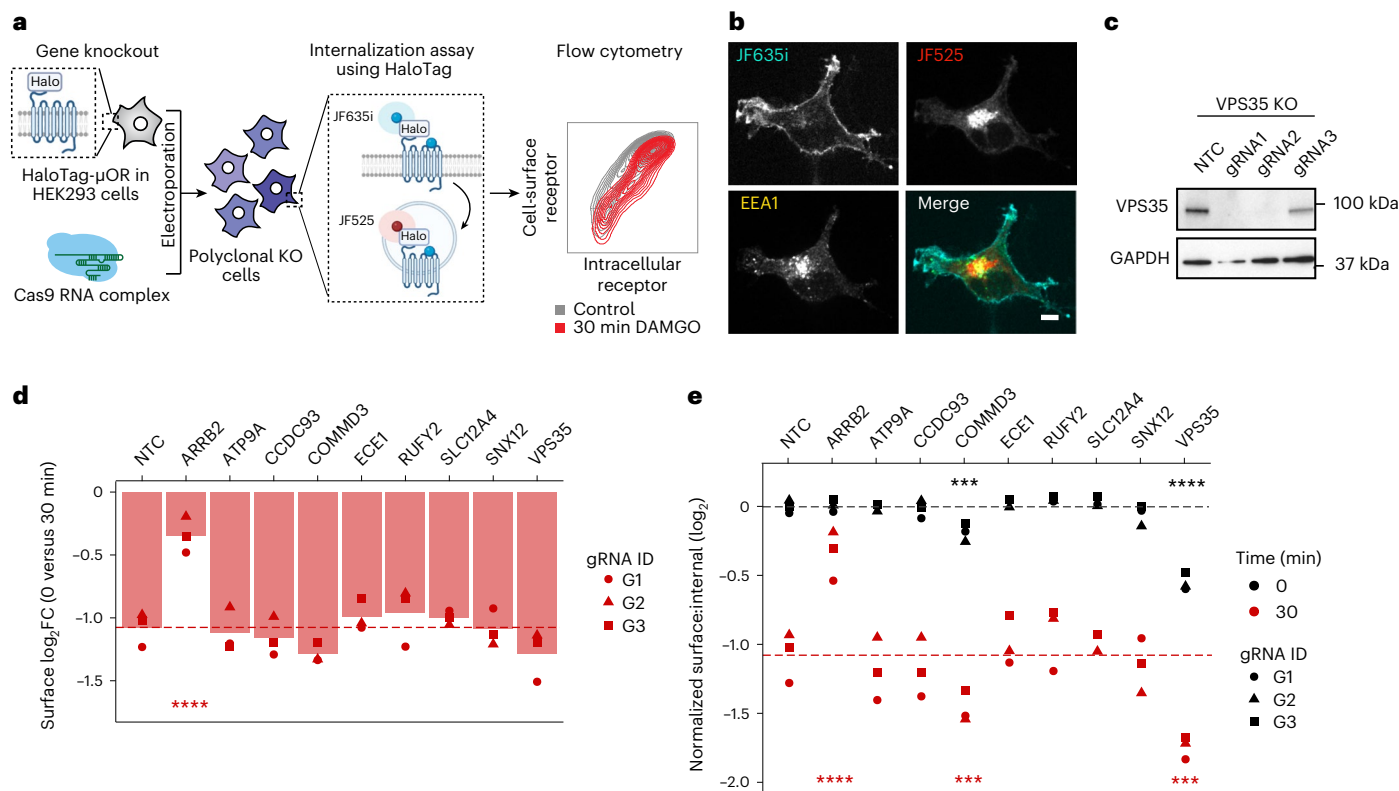


Fig. 4 | Knockouts of VPS35 and COMMD3 change cellular distribution of the μ OR. **a**, Targeted CRISPR knockout screen to probe for μ OR cell-surface expression, internalization and trafficking. The μ OR is stably expressed in HEK293 cells with an N-terminally fused HaloTag. Polyclonal knockout cell lines are generated by nucleofection of CRISPR ribonucleoprotein complexes. Effects of gene knockout on μ OR cell-surface expression and internalization is assessed by receptor activation with DAMGO for 30 min followed by covalent binding of cell-impermeable (JF635i) and permeable (JF525) fluorescent dyes to HaloTag, to differentially label the μ OR at the cell surface and intracellular compartments. **b**, Imaging cell-surface and intracellular μ OR using cell-permeable and impermeable Halo dyes. JF635i was used to mark the receptor on the cell surface, JF525 was used to label the intracellular receptor. Colocalization of the intracellular μ OR with endosomes was marked using an anti-EEA1. Scale bar, 10 μ m. **c**, Confirmation of gene knockout for three different guide RNAs

targeting VPS35. GAPDH is used as loading control. $n = 3$ independent biological replicates, representative example shown. **d**, Bar plot depicts loss in cell-surface μ OR upon activation with 10 μ M DAMGO for 30 min and in the context of CRISPR-based knockout of selected genes and NTC. Line depicts the average cell-surface μ OR loss for the NTC. For each gene, three gRNAs were used and for each guide three biological replicates were summarized. Two-tailed t statistics, **** P (ARRB2) = 1×10^{-5} . **e**, Plot depicts the normalized ratio comparing the population of the receptors at the cell surface and intracellularly in the presence and absence of μ OR activation with 10 μ M DAMGO for 30 min. Lines depicts the average normalized cell surface-to-intracellular ratio for NTC. For each gene, three guide RNAs (gRNA) were used and for each guide three biological replicates were summarized. Two-tailed t statistics, **** P (ARRB2, 30 min) = 0.00005, *** P (COMMD3, 0 min) = 2×10^{-4} , ** P (COMMD3, 30 min) = 0.01, **** P (VPS35, 0 min) = 2×10^{-11} , *** P (VPS35, 30 min) = 2×10^{-4} .

GPCRs stimulate or inhibit cAMP production by coupling to G_s and G_i subclass G proteins, respectively. Using isoproterenol to activate endogenous G_s -coupled β -adrenergic receptors in HEK293 cells, we verified the characteristic G_s -mediated cAMP response, as defined by elevation of cAMP to a peak within several minutes followed by a decrease or desensitization phase in the prolonged presence of agonist (Fig. 6a, left, black curve). Using DAMGO to activate exogenously expressed μ OR (blue) or somatostatin (SST) to activate endogenous G_i -coupled somatostatin receptors (green) in HEK293 cells, we verified inhibition of the cAMP response throughout its time course and affecting the time-integrated response (Fig. 6a, right). DAMGO inhibited the response more strongly than SST, consistent with recombinant μ OR being overexpressed.

We then applied the cAMP assay to investigate effects of EYA4 and KCTD12 on both G_s - and G_i -mediated signaling. Depleting endogenous EYA4 by CRISPR-mediated gene knockout (EYA4 KO; Extended Data Fig. 8) suppressed the isoproterenol-induced cAMP response over its full time course (Fig. 6b, left, open circles), resulting in a significant reduction of the integrated cAMP response (Fig. 6b, right). A similar effect was observed in an independent KO cell clone (Extended Data Fig. 9a,b) as well as in a polyclonal population of cells where EYA4 was

partially knocked out using CRISPR (Supplementary Fig. 1a,b). Notably, the magnitude of inhibition produced by EYA4 KO was comparable to that produced by SST in control (NT) cells (compare with Fig. 6a,b), suggesting that this effect is in a functionally relevant range. However, EYA4 KO did not prevent the effect of G_i , because both SST and DAMGO were still able to further suppress the Iso-induced cAMP response in EYA4 KO cells, and do so to a higher degree than in NT cells (Fig. 6c and Supplementary Fig. 1a,b). The overall effects of EYA4 on G-protein signaling cannot be fully explained by modulation of G_i alone, as PTX treatment did restore the effect on G_i -mediated cAMP inhibition (Extended Data Fig. 9c, left), but did not restore G_s -mediated cAMP production to NT levels in EYA4 KO cells (Extended Data Fig. 9c, right).

KCTD12 KO did not detectably change the peak cAMP response, but it produced an apparent slowing of desensitization. This was a small effect, however, which did not result in a significant change in the integrated cAMP response (Fig. 6d). A similar but more pronounced effect was observed in the second KCTD12 KO clone, resulting in a significant increase of the integrated isoproterenol-induced cAMP response (Extended Data Fig. 9d). KCTD12 KO also appeared to enhance G_i -mediated inhibition of the cAMP response through endogenous SST receptors, and this effect was significant in both KO clones while

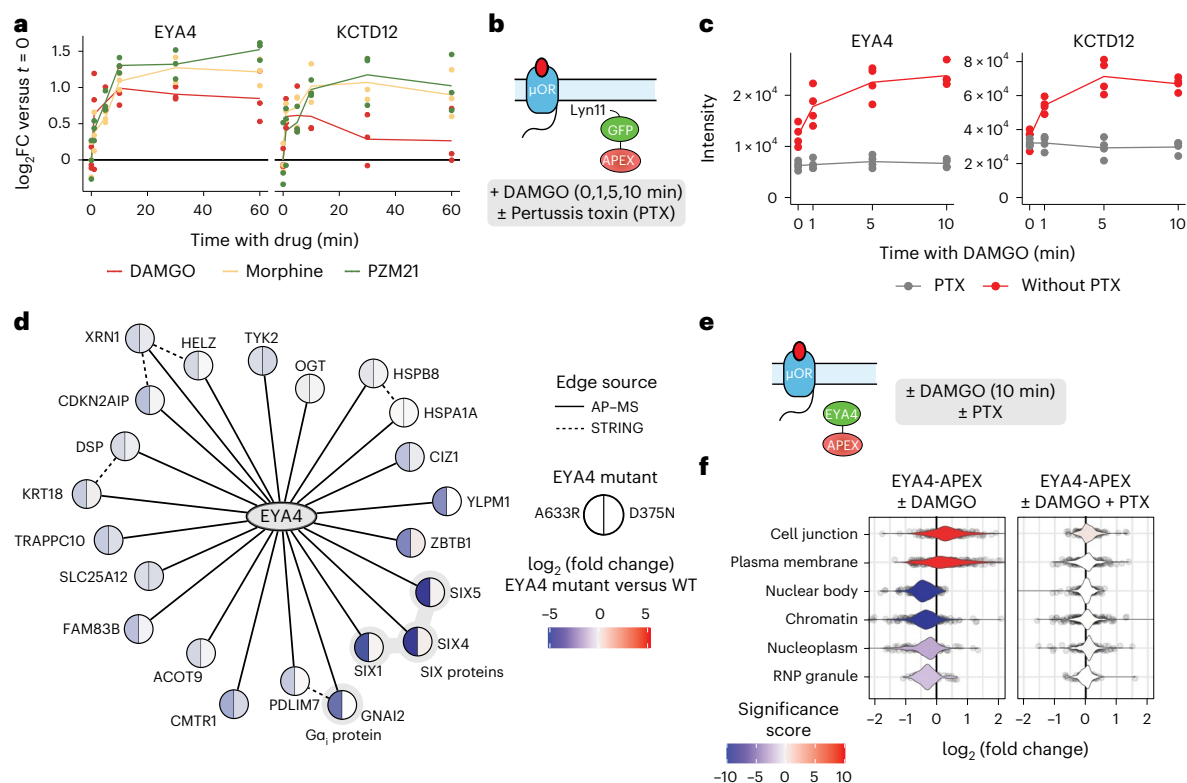


Fig. 5 | EYA4 and KCTD12 are recruited in the μ OR proximal interaction network in a $G_{\alpha i}$ activity-dependent manner. **a, Temporal profile for KCTD12 and EYA4. Line charts represent the \log_2 FC over the time course of receptor activation with DAMGO (red), morphine (yellow) and PZM21 (green) after data detrending. Data from three biological replicates are presented. **b**, Schematic of APEX2-based proximity labeling of the plasma membrane spatial reference construct (PM-APEX2) was performed in a cell line expressing the μ OR in the presence and absence of the $G_{\alpha i}$ inhibitor PTX and after activation of μ OR using DAMGO. **c**, Line charts depict protein intensity for KCTD12 and EYA4 in PM-APEX2 experiment determined by quantitative MS over the DAMGO time course in the**

presence (gray) and absence (red) of PTX. Data from four biological replicates are presented. **d**, Interaction network of high-confidence interactors of EYA4 determined by affinity purification. Split nodes indicate protein abundance differences for the high-confidence interactors upon introduction of SIX-binding mutant (A633R) and phosphatase-dead mutant (D375N). Data from three biological replicates are presented as mean. **e**, APEX2-based proximity labeling of EYA4 was performed in a cell line expressing the μ OR in the presence and absence of the $G_{\alpha i}$ inhibitor PTX and after activation of the μ OR using DAMGO. **f**, Gene-set enrichment analysis (GSEA) in \log_2 FC depicted in Extended Data Fig. 8 using the location-specific sets of proteins defined in Human Cell Map.

varying in degree between them (Fig. 6e and Extended Data Fig. 9e). We did not observe a comparable effect when G_i -mediated inhibition was elicited through overexpressed μ OR (Extended Data Fig. 9f,g), but were able to elicit the converse effect, reduced μ OR-mediated inhibition, when KCTD12 was overexpressed together with the μ OR and utilizing concentration–response analysis to assess signaling (Extended Data Fig. 9h). Previous studies indicate that KCTD12 regulates signaling primarily through interactions with $G\beta\gamma$ subcomplexes, whereas cAMP production in HEK293 cells is regulated both by G_{α} and $G\beta\gamma$ subunits. Thus, we next tested regulation of overexpressed GIRK channels as a more direct readout of signaling via $G\beta\gamma$. Using DAMGO to elicit $G\beta\gamma$ release through the μ OR, we verified a rapid inward current followed by a slow 20–40% desensitization over the course of 60 s. KCTD12 KO did not detectably affect the initial current amplitude (Extended Data Fig. 10a) elicited by DAMGO, but it decreased either the speed (Fig. 6f) or extent of desensitization (Extended Data Fig. 10b), depending on the agonist dose applied. Conversely, overexpression of KCTD12 accelerated GIRK current desensitization (Extended Data Fig. 10c).

Together, these results indicate that both EYA4 and KCTD12 indeed impact cellular G -protein responses, but their effects differ: EYA4 enhances the acute $G_{\alpha s}$ -mediated cAMP elevation in a manner that is consistent with it binding $G_{\alpha i}$, but probably involving additional homeostatic adaptation(s) of the signaling network. KCTD12 promotes signal desensitization after the peak, and it impacts both $G_{\alpha s}$ - and G_i -mediated signaling in a manner consistent with it binding $G\beta\gamma$.

Discussion

A fundamental question for the μ OR, and generally for GPCRs, is whether additional proteins beyond known signal transducers (for example, G proteins, GRKs and arrestins) are recruited into the μ OR proximal interaction network to mediate the receptor's cellular effects. To start addressing this question and to enable systematic characterization of the μ OR cellular response on the basis of receptor trafficking and its interaction networks, we advanced the previously developed GPCR-APEX methodology. We performed GPCR-APEX for the μ OR after activation with three chemically diverse agonists, DAMGO, morphine and PZM21, to determine global changes in the proximal proteome of the receptor over the time course of activation (Fig. 1).

Previous challenges of the GPCR-APEX methodology included: (1) the data complexity resulting from receptor trafficking to multiple compartments; and (2) the lack of computational approaches to deconvolve proximity labeling data into their constituent parts—spatial bystanders and functional proximal interaction networks. We introduce a computational framework addressing these challenges by modeling receptor trafficking on the basis of quantitative protein measurements in the proximity labeling data (Fig. 2), requiring minimal knowledge of the receptor trafficking itinerary and its kinetics. This substantially advances previous work, which required measurement of receptor trafficking with complementary methods⁸. The computational framework requires a priori selection of spatial references based either on prior knowledge or on information inherent in the GPCR-APEX

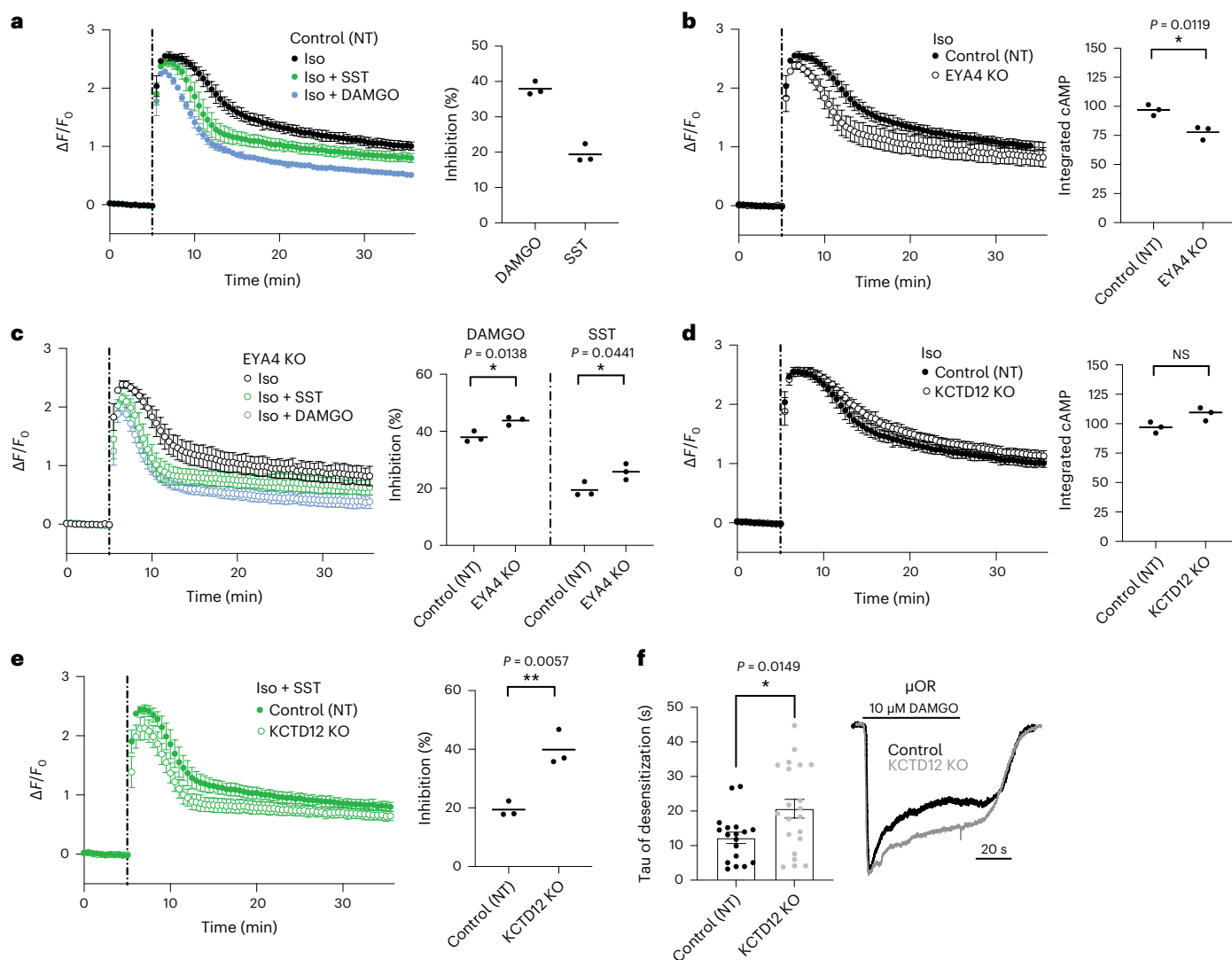


Fig. 6 | EYA4 and KCTD12 modulate G-protein-mediated signaling. a, cAMP activity in HEK293 nontargeting control (NT) cells stably expressing the μ OR. Change in fluorescence intensity of cAMP biosensor upon stimulation with 100 nM isoproterenol (Iso) without (black) and with co-application of 1 μ M SST (green) or 10 μ M DAMGO (blue) is plotted. $n = 3$ biological replicates. **b**, cAMP activity in control (closed) and EYA4 KO (open) cells upon stimulation with Iso. Control curve repeated from panel **a**. $n = 3$ biological replicates, $*P = 0.0119$. **c**, cAMP activity in EYA4 KO cells upon stimulation with Iso, with and without co-application of SST or DAMGO. Percentage inhibition for control (NT) repeated from panel **a**. Iso curve repeated from panel **b**. $n = 3$ biological replicates, $*P(\text{DAMGO}) = 0.0138$, $*P(\text{SST}) = 0.0441$. **d**, cAMP activity in control (closed) and KCTD12 KO (open) HEK293 cells stably expressing the μ OR upon stimulation

with Iso. Control curve repeated from panel **a**. $n = 3$ biological replicates. **e**, cAMP activity in control and KCTD12 KO cells upon stimulation with Iso and SST. Percentage inhibition for control repeated from panel **a**. $n = 3$, $**P = 0.0057$. For all cAMP panels, data represent $n = 3$ biological replicates, shown as individual data points or mean \pm s.d., and significance was determined by unpaired, two-tailed t -test. **f**, Quantification of the tau of desensitization of μ OR-mediated GIRK currents over 60 s 10 μ M DAMGO application, in control and KCTD12 KO HEK cells. Each point represents an individual cell. Unpaired, two-tailed t -test, $*P = 0.0149$. Error bars represent s.e.m. (left). Representative whole-cell patch clamp recording displaying GIRK currents mediated by μ OR activation over 60 s DAMGO, in control and KCTD12 KO cells (right). NS, not significant.

data and their parallel processing with the GPCR-APEX samples. The spatial references allow estimating the proximity labeling background proteome followed by calculation of coefficients for subcellular compartments. The compartment-specific proximity labeling background proteome is determined without expression or activation of the μ OR, assuming that most of the compartmental proteome does not change upon receptor activation. Notably, while the location coefficients do not provide an absolute measure of the receptor at a given subcellular location, they estimate its relative distribution within the cell and how it dynamically changes upon receptor activation. Nevertheless, we demonstrate that the coefficients provide the means to subtract most location-specific trends from the GPCR-APEX datasets.

Applying this framework to the μ OR, we provide a comprehensive dataset of the proximal protein environment of the receptor produced by its activation with the opioid peptide agonist DAMGO, the opiate alkaloid partial agonist morphine and the chemically distinct ‘biased’ partial agonist PZM21. Striking ligand-dependent trafficking behavior of the μ OR emerged with subcellular resolution: DAMGO provoked strong internalization and subsequent trafficking, which was reduced by morphine, and essentially undetectable by PZM21. PZM21 emerged from a structure-based effort to develop agonists functionally selective for $G\alpha_i$ (ref. 10), leading to a compound with strong analgesic effects and with reduced side effects, which are otherwise characteristic of μ OR agonists. Whereas the precise mechanistic bases of the apparent

functional selectivity of PZM21 and other biased agonists²¹ remains controversial^{22,23}, the differential μ OR trafficking when activated by PZM21 supports differentiation from agonists like DAMGO and even morphine. The proteomic-based characterization of trafficking and downstream protein engagement offers arguably a holistic way to investigate cellular effects of novel ligands, aiding the development of functionally selective molecules in GPCR signaling.

We utilized the spatial information from our computational framework to detrend the proximity labeling dataset for location-specific effects (Fig. 2). This process enriched for functionally relevant proteins in the receptor interaction network (Fig. 3), exemplified by well-characterized interactors functioning in GPCR signaling and trafficking, such as ARRB2 and members of the Retromer and WASH complexes. Additionally, we discovered novel proteins regulating μ OR signaling and trafficking, such as COMMD3 and VPS35, DAMGO-specific proteins regulating μ OR cellular distribution and EYA4 and KCTD12, common proximal interactors across all three ligands regulating receptor signaling. While our study was conducted in HEK293 cells lacking endogenous μ OR expression, we captured 95% of the μ OR proximal interactors upon DAMGO activation in μ OR-expressing SH-SY5Y neuroblastoma cells (Extended Data Fig. 6). Impressively, we observed very similar kinetics for most proteins, including ARRB2, VPS35, EYA4 and VPS35, between the two cell systems, suggesting conservation of the fundamental machinery regulating GPCR signaling and trafficking. However, differences were observed in these two cell types, indicating that results from HEK293 cells may not extrapolate directly to neurons without further experiments. Furthermore, the data detrending process based on spatial references is not without limitations. It assumes that the GPCR-APEX construct and the spatial references result in similar protein labeling patterns at a given location, which might not hold true for all proteins in the dataset, given that GPCRs can traffic to multiple compartments and potentially reside in different subcellular microdomains compared to the spatial references. Therefore, functional characterization and/or validation in relevant cell systems is essential to support any hypotheses derived from the proximal interaction networks.

Highlighting the capacity of the GPCR-APEX/proteomics pipeline to discover novel functional interactors of GPCRs, we identify COMMD3 and VPS35 as ligand-specific μ OR regulators. Knockout of COMMD3 and VPS35, two proximal μ OR interactors predominantly upon activation with DAMGO, shifts the receptor distribution from the cell surface to intracellular compartments (Fig. 4). These observations are consistent with COMMD3 and VPS35 acting at a postendocytic step of μ OR trafficking. VPS35 is a subunit of the endosomal sorting complex Retromer, and COMMD3 is a subunit of the Commander sorting complex²⁴. The Retromer and Commander complexes mediate endosomal sorting and recycling of a largely nonoverlapping set of membrane proteins. Retromer binds membrane proteins with Ω x[L/M/V] (where Ω is any aromatic amino acid) or, when in complex with SNX27, [-][ϕ]x[-][S/T]x ϕ -COOH motifs (where - is any negatively charged amino acid)²⁵. For example, SNX27/Retromer has been shown to mediate endosomal recycling of multiple GPCRs, including B2AR and PTH1R^{26–29}. Conversely, the Commander complex consists of two subcomplexes (CCC and Retriever) and, via Retriever, bind membrane proteins with an NPxY motif^{30,31}. Intriguingly, the recycling motif in μ OR, LENLE, does not match the motifs bound by either Retromer or Retriever. Thus, our results add to the emerging view that multiple sorting interactions occur in the endosomal limiting membrane, necessitating further investigation into the function of VPS35 and COMMD3 in endosomal trafficking of μ OR.

We also discovered EYA4 and KCTD12 as components in the proximal interaction network of the μ OR recruited upon activation by all ligands and in a G_i -dependent manner (Fig. 5). Our results suggest that these proximal network components each produces distinct effects on cellular signaling by GPCRs. Our knockout data suggest dual functional

effects of EYA4: (1) enhancing G_s -mediated stimulation of cytoplasmic cAMP; and (2) limiting the ability of G_i to suppress this response. This second effect may arise from the preferential binding of EYA4 to activated G_{α_i} , as indicated by our affinity purification (AP)–MS data. It is conceivable that the first effect could be mediated by the same mechanism if basal G_i tone is high. We think this is not the case, however, because the Iso-induced cAMP elevation is retained in cells pretreated with PTX, a manipulation that should prevent regulation by G_i altogether (Extended Data Fig. 9c). Accordingly, we speculate that EYA4 has two functional signaling effects: it limits G_i signaling, probably by binding to activated G_{α_i} , and it enhances G_s -mediated stimulation through an additional effect on cellular cAMP homeostasis that remains to be delineated. While we demonstrate activity-dependent recruitment of EYA4 in μ OR proximity in SH-SY5Y neuroblastoma cells (Extended Data Fig. 6), the impact of EYA4 on G_i signaling in intact neurons remains unexplored, presenting an important future direction of study.

KCTD12 is a well-characterized auxiliary subunit for GABA_A receptors that regulates the rise time and duration of GIRK signaling by competitive binding to $G\beta$ subunits^{18–20}. Our study supports the hypothesis that KCTD12 can impact G-protein-mediated signaling through $G\beta$ for other receptors, as previously suggested¹⁹. However, unlike GABA_A receptors, our data indicate that KCTD12 is not constitutively bound to the C-terminal tail of the μ OR. Instead, KCTD12 appears to be directly recruited to the dissociated $G\beta$ subunit following receptor activation. A plausible model is that KCTD12 sequesters $G\beta$ subcomplexes produced under agonist-induced conditions, depleting G-protein heterotrimers available for reactivation after prolonged agonist exposure. While other possibilities cannot be excluded at present, and we note recent evidence for an additional effect of KCTD12 on adenylyl cyclase activity³², this simple model is attractive because it is sufficient to explain KCTD12 affecting both cAMP and GIRK signaling, as well as enhancing desensitization without changing the acute agonist response. Notably, as EYA4 and KCTD12 interact with dissociated G-protein subunits rather than the receptor itself, we conclude that GPCR-APEX is sufficiently sensitive to enable exploration of the proximal interaction network engaged and regulated by GPCRs beyond the level of direct receptor interactions.

Overall, our proximity labeling data from HEK cells does not suggest proteins uniquely associating with the μ OR upon stimulation with morphine and PZM21, but rather suggests that the proximal interaction networks of the morphine- and PZM21-activated μ OR represent a subset of the DAMGO network, probably differing in interactors involved in receptor endocytosis and trafficking. However, ligand-specific interactors that were either not captured by the APEX-based proximity labeling approach or are not expressed in HEK293T cells and might only be captured in other cell systems endogenously expressing the μ OR cannot be ruled out at present.

An earlier study using APEX-based proximity labeling proteomics for μ OR discovered that morphine-activated, but not DAMGO-activated, μ OR led to increased labeling of desmosomal proteins³³. A model was proposed in which the proximity to desmosomes controls morphine-mediated activation of sustained ERK within the cytoplasm³³. While our data indicate differences in biotin labeling of desmosomal proteins comparing stimulation with DAMGO and morphine, we hypothesize that these observations rather stem from ligand-dependent differences in receptor trafficking, leading to decreased labeling of plasma membrane proteins for the DAMGO-activated μ OR.

Taken together, the presented approach is broadly applicable to assess and compare ligand-specific effects on GPCR activation. To our knowledge, this is the first methodology capable of simultaneously capturing the multiple layers of receptor activation–location and interaction networks in an unbiased and medium-throughput fashion. As such we envisage that its application will prove to be key in informing hypothesis-driven exploration of the molecular mechanisms for

how chemically distinct ligands can evoke different cellular responses, but also in drug discovery efforts to characterize and prioritize novel receptor ligands for in vivo testing.

Online content

Any methods, additional references, Nature Portfolio reporting summaries, source data, extended data, supplementary information, acknowledgements, peer review information; details of author contributions and competing interests; and statements of data and code availability are available at <https://doi.org/10.1038/s41589-024-01588-3>.

References

1. Kieffer, B. L. & Evans, C. J. Opioid receptors: from binding sites to visible molecules in vivo. *Neuropharmacology* **56**, 205–212 (2009).
2. Corder, G., Castro, D. C., Bruchas, M. R. & Scherrer, G. Endogenous and exogenous opioids in pain. *Annu. Rev. Neurosci.* **41**, 453–473 (2018).
3. Hilger, D., Masureel, M. & Kobilka, B. K. Structure and dynamics of GPCR signaling complexes. *Nat. Struct. Mol. Biol.* **25**, 4–12 (2018).
4. von Zastrow, M. Proteomic approaches to investigate regulated trafficking and signaling of G protein-coupled receptors. *Mol. Pharmacol.* **99**, 392–398 (2021).
5. Degrandmaison, J., Rochon-Haché, S., Parent, J.-L. & Gendron, L. Knock-in mouse models to investigate the functions of opioid receptors in vivo. *Front. Cell. Neurosci.* **16**, 807549 (2022).
6. Rhee, H.-W. et al. Proteomic mapping of mitochondria in living cells via spatially restricted enzymatic tagging. *Science* **339**, 1328–1331 (2013).
7. Hung, V. et al. Proteomic mapping of the human mitochondrial intermembrane space in live cells via ratiometric APEX tagging. *Mol. Cell* **55**, 332–341 (2014).
8. Lobingier, B. T. et al. An approach to spatiotemporally resolve protein interaction networks in living cells. *Cell* **169**, 350–360 (2017).
9. Paek, J. et al. Multidimensional tracking of GPCR signaling via peroxidase-catalyzed proximity labeling. *Cell* **169**, 338–349 (2017).
10. Manglik, A. et al. Structure-based discovery of opioid analgesics with reduced side effects. *Nature* **537**, 185–190 (2016).
11. McPherson, J. et al. μ -Opioid receptors: correlation of agonist efficacy for signalling with ability to activate internalization. *Mol. Pharmacol.* **78**, 756–766 (2010).
12. Lau, E. K. et al. Quantitative encoding of the effect of a partial agonist on individual opioid receptors by multisite phosphorylation and threshold detection. *Sci. Signal.* **4**, ra52 (2011).
13. Choi, M. et al. MSstats: an R package for statistical analysis of quantitative mass spectrometry-based proteomic experiments. *Bioinformatics* **30**, 2524–2526 (2014).
14. Ehrlich, A. T. et al. Biased signaling of the mu opioid receptor revealed in native neurons. *iScience* **14**, 47–57 (2019).
15. Hegde, R. S., Roychoudhury, K. & Pandey, R. N. The multi-functional eyes absent proteins. *Crit. Rev. Biochem. Mol. Biol.* **55**, 372–385 (2020).
16. Fan, X. et al. The alpha subunits of G₂ and G₁ interact with the eyes absent transcription cofactor Eya2, preventing its interaction with the six class of homeodomain-containing proteins. *J. Biol. Chem.* **275**, 32129–32134 (2000).
17. Embry, A. C., Glick, J. L., Linder, M. E. & Casey, P. J. Reciprocal signaling between the transcriptional co-factor Eya2 and specific members of the Gai family. *Mol. Pharmacol.* **66**, 1325–1331 (2004).
18. Schwenk, J. et al. Native GABA_B receptors are heteromultimers with a family of auxiliary subunits. *Nature* **465**, 231–235 (2010).
19. Turecek, R. et al. Auxiliary GABA_B receptor subunits uncouple G protein $\beta\gamma$ subunits from effector channels to induce desensitization. *Neuron* **82**, 1032–1044 (2014).
20. Zheng, S., Abreu, N., Levitz, J. & Kruse, A. C. Structural basis for KCTD-mediated rapid desensitization of GABA_B signalling. *Nature* **567**, 127–131 (2019).
21. DeWire, S. M. et al. A G protein-biased ligand at the μ -opioid receptor is potently analgesic with reduced gastrointestinal and respiratory dysfunction compared with morphine. *J. Pharmacol. Exp. Ther.* **344**, 708–717 (2013).
22. Kliewer, A. et al. Morphine-induced respiratory depression is independent of β -arrestin2 signalling. *Br. J. Pharmacol.* **177**, 2923–2931 (2020).
23. Bachmutsky, I., Wei, X. P., Durand, A. & Yackle, K. β -arrestin 2 germline knockout does not attenuate opioid respiratory depression. *eLife* **10**, e62552 (2021).
24. Cullen, P. J. & Steinberg, F. To degrade or not to degrade: mechanisms and significance of endocytic recycling. *Nat. Rev. Mol. Cell Biol.* **19**, 679–696 (2018).
25. Yong, X., Mao, L., Seaman, M. N. J. & Jia, D. An evolving understanding of sorting signals for endosomal retrieval. *iScience* **25**, 104254 (2022).
26. Lauffer, B. E. L. et al. SNX27 mediates PDZ-directed sorting from endosomes to the plasma membrane. *J. Cell Biol.* **190**, 565–574 (2010).
27. Temkin, P. et al. SNX27 mediates retromer tubule entry and endosome-to-plasma membrane trafficking of signalling receptors. *Nat. Cell Biol.* **13**, 715–721 (2011).
28. McGarvey, J. C. et al. Actin-sorting nexin 27 (SNX27)-retromer complex mediates rapid parathyroid hormone receptor recycling. *J. Biol. Chem.* **291**, 10986–11002 (2016).
29. Chan, A. S. M. et al. Sorting nexin 27 couples PTHR trafficking to retromer for signal regulation in osteoblasts during bone growth. *Mol. Biol. Cell* **27**, 1367–1382 (2016).
30. McNally, K. E. et al. Retriever is a multiprotein complex for retromer-independent endosomal cargo recycling. *Nat. Cell Biol.* **19**, 1214–1225 (2017).
31. Healy, M. D. et al. Structure of the endosomal Commander complex linked to Ritscher–Schinzel syndrome. *Cell* **186**, 2219–2237 (2023).
32. Muntean, B. S. et al. Members of the KCTD family are major regulators of cAMP signaling. *Proc. Natl Acad. Sci. USA* **119**, e2119237119 (2022).
33. Civciristov, S. et al. Ligand-dependent spatiotemporal signaling profiles of the μ -opioid receptor are controlled by distinct protein-interaction networks. *J. Biol. Chem.* **294**, 16198–16213 (2019).

Publisher's note Springer Nature remains neutral with regard to jurisdictional claims in published maps and institutional affiliations.

Springer Nature or its licensor (e.g. a society or other partner) holds exclusive rights to this article under a publishing agreement with the author(s) or other rightsholder(s); author self-archiving of the accepted manuscript version of this article is solely governed by the terms of such publishing agreement and applicable law.

© The Author(s), under exclusive licence to Springer Nature America, Inc. 2024

Methods

Mammalian cell culture conditions

HEK293 cells were obtained from the American Type Culture Collection (ATCC CRL-1583), cultured in Dulbecco's modified Eagle's medium (DMEM, GIBCO or Fisher Scientific), supplemented with 10% fetal bovine serum (FBS, UCSF Cell Culture Facility) and maintained at 37 °C in a 5% CO₂ humidified incubator. HEK293 cells stably expressing APEX2-tagged μ OR (mouse) and APEX2-tagged spatial reference constructs were selected with 500 μ g ml⁻¹ G418 and maintained in 100 μ g ml⁻¹ G418. Transfections were performed using Lipofectamine 2000 (Invitrogen) or Lipofectamine 3000 (Invitrogen) for complementary DNA (2 μ l of Lipofectamine per 1 μ g of DNA). For transient DNA expression, cells were transfected 24 or 48 h before experiments. For electrophysiology measurements, cells were seeded on poly-L-lysine-coated 18-mm coverslips. Transfections were performed using Lipofectamine 2000 (Invitrogen).

SH-SY5Y cells were obtained from the American Type Culture Collection (ATCC CRL-2266) and cultured in DMEM/Ham's F-12 with L-glutamine (Cytiva), supplemented with 10% FBS (Thermo Fisher) and PenStrep (Corning) and maintained at 37 °C in a 5% CO₂ humidified incubator. APEX2-tagged μ OR (human) was stably expressed using lentiviral transduction followed by selection with 2 μ g ml⁻¹ puromycin.

APEX reaction, biotinylated protein enrichment and preparation for mass spectrometry analysis

For the μ OR-APEX2 experiments the following method was used to perform biotinylation, enrichment and prepare the samples for MS analysis. First, 500 μ M biotin-phenol was preincubated with cells expressing μ OR-APEX2 for 30 min at 37 °C. Then, 10 μ M DAMGO ([D-Ala², N-Me-Phe⁴, Gly⁵-ol]-enkephalin acetate salt, Sigma-Aldrich), morphine (morphine sulfate, Sigma-Aldrich) or PZM21 (synthesized by Enamine at 98% purity as tested by NMR and LC-MS) was added for the noted period of time. For the spatial references, cells expressing PM-APEX2, Endo-APEX2 and Lyso-APEX2 were incubated with 500 μ M biotin-phenol for 30 min at 37 °C; no agonists were added to these cells. Immediately before use, H₂O₂ was diluted to 2 mM final in room-temperature media (DMEM + 10% FBS). APEX2 labeling was initiated by 1:1 mixing of the H₂O₂-containing media (1 mM H₂O₂ final) with the biotin-phenol-containing media at room temperature. The labeling reaction was allowed to continue for 30 s, media were removed and the cells were washed three times in ice-cold quenching buffer (TBS supplemented with 1 mM CaCl₂, 10 mM sodium ascorbate, 1 mM sodium azide and 1 mM Trolox). Cells were incubated in quenching buffer for 20 min on ice, quenching buffer was removed and cells were lysed in RIPA (50 mM Tris, 150 mM NaCl, 1% Triton X-100, 0.5% deoxycholate, 0.1% SDS, pH 7.4) supplemented with 10 mM sodium ascorbate and protease inhibitors (Roche Complete). Samples were briefly sonicated, spun down at 10,000g for 10 min, the supernatant was applied to streptavidin agarose resin (Thermo) and incubated overnight at 4 °C.

Streptavidin agarose resin was washed two times in RIPA buffer (50 bed volumes per wash), four times in TBS (50 bed volumes per wash), one time in 50 mM NH₄HCO₃, 3 M urea (1 bed volume per wash). Samples were reduced on resin by adding TCEP (5 mM final) and incubating, with orbital shaking, for 30 min at 55 °C. Samples were alkylated by adding iodoacetamide (10 mM final), covered from light and with orbital shaking, for 20 min at room temperature. The reaction was quenched upon addition of DTT (20 mM final). The streptavidin agarose resin was spun down and the buffer exchanged to 50 mM NH₄HCO₃, 2 M urea. Biotinylated proteins were cleaved on resin by the incubation of trypsin overnight at 37 °C (1 μ g trypsin per 20 μ l streptavidin agarose). Following proteolysis, the resin was spun down by centrifugation at 1,000g for 1 min and the supernatant collected. The resins were washed twice with 50 mM NH₄HCO₃, 2 M urea and this material was pooled with the first supernatant. The sample was acidified with TFA. NEST C18 MacroSpin columns were used to desalt the peptide sample for MS analysis.

For the PM-APEX2 samples, EYA4-APEX2 samples and μ OR-APEX2 samples derived from SH-SY5Y cells the following method was used to perform biotinylation, enrichment and to prepare the samples for MS analysis. HEK293 cells expressing the μ OR (human) and either the PM-APEX2 or EYA4-APEX2 construct were incubated with 500 μ M biotin-phenol at 37 °C for 30 min. Then, 10 μ M DAMGO was added for three different time points including 1, 5 and 10 min for PM-APEX2, and 10 min for EYA4-APEX2. For the PTX treatment condition, cells were preincubated with 100 ng ml⁻¹ pertussis toxin for 18 h before DAMGO treatment. APEX labeling was initiated by 1:1 mixing of the H₂O₂-containing media (1 mM H₂O₂ final) with the biotin-phenol-containing media at room temperature. After 45 s of the biotinylation reaction, the cells were washed three times (1 min each) with ice-cold quenching buffer (PBS supplemented with 10 mM sodium ascorbate, 10 mM sodium azide and 5 mM Trolox). Cells were then collected in 8 ml quench buffer and pelleted by centrifugation at 4 °C for 10 min at 3,000g. For cell lysis, cells were homogenized using probe sonication in RIPA (50 mM Tris, 150 mM NaCl, 1% Triton X-100, 0.25% sodium deoxycholate, 0.25% SDS, pH 7.4) supplemented with 10 mM sodium ascorbate, 10 mM sodium azide, 5 mM Trolox, 1 mM DTT and protease inhibitors (Roche Complete). To remove the cell debris, cell lysate was centrifuged at 10,000g for 10 min, and the supernatant was taken for streptavidin enrichment of biotinylated proteins.

The enrichment of biotinylated proteins was automated with the KingFisher Flex (Thermo Fisher Scientific). Supernatants were incubated at 4 °C for 18 h with magnetic streptavidin beads (Pierce Streptavidin Magnetic Beads, Thermo Fisher Scientific), which were prewashed twice with RIPA buffer. Following incubation, beads were washed three times with RIPA buffer, one time with 1 M KCl, one time with 0.1 M Na₂CO₃, one time with 2 M urea in 50 mM Tris-HCl (pH 8) buffer and two times with 50 mM Tris-HCl (pH 8) buffer. Beads were maintained in 200 μ l of 2 M urea in 50 mM Tris-HCl (pH 8) buffer for on-bead digestion of proteins. Samples were reduced with 5 mM TCEP at 37 °C for 30 min, followed by alkylation with 5 mM 2-iodoacetamide (IAA) at room temperature for another 30 min, which was quenched by addition of DTT (5 mM final). For tryptic digestion, 1 μ g trypsin was added to beads and incubated with shaking at 37 °C for 4 h. Supernatants were taken and saved for desalting using NEST C18 MicroSpin columns.

Unbiased mass spectrometric data acquisition and protein quantification for APEX samples

Digested peptide mixtures were analyzed by LC-MS/MS on a Thermo Scientific Orbitrap Fusion Tribrid mass spectrometry system equipped with a Proxeon Easy nLC1000 ultra-high-pressure liquid chromatography and autosampler system. Samples were injected onto a C18 column (25 cm \times 75 μ m internal diameter (ID) packed with ReproSil-Pur-C18AQ 1.9 μ m particles) in 0.1% formic acid and then separated with an 80 min gradient from 5% to 30% acetonitrile (ACN) in 0.1% formic acid (FA) at a flow rate of 300 nl min⁻¹. The mass spectrometer collected data in a data-dependent fashion, collecting one full scan in the Orbitrap at 120,000 resolution, followed by collision-induced dissociation MS/MS scans in the dual linear ion trap with a maximum cycle time of 3 s between each full scan. Dynamic exclusion was enabled for 30 s with a repeat count of 1. Charge-state screening was employed to reject analysis of singly charged species or species for which a charge could not be assigned.

The raw data were analyzed using the MaxQuant algorithm (v.1.5.5.1) for the identification and quantification of peptides and proteins³⁴. Data were searched against the SwissProt Human database (downloaded January 2017), augmented with the mouse Oprm and the APEX2 sequence, concatenated to a decoy database where each sequence was randomized to estimate the false discovery rate (FDR). Variable modifications were allowed for methionine oxidation and protein N-terminus acetylation. A fixed modification was indicated for

cysteine carbamidomethylation. Full trypsin specificity was required. The first search was performed with a mass accuracy of ± 20 parts per million and the main search was performed with a mass accuracy of ± 4.5 parts per million. A maximum of five modifications and two missed cleavages were allowed per peptide. The maximum charge was set to +7. Individual peptide mass tolerances were allowed. For MS/MS matching, the mass tolerance was set to 0.8 Da and the top eight peaks per 100 Da were analyzed. MS/MS matching was allowed for higher charge states, water and ammonia loss events. The data were filtered to obtain a peptide, protein and site-level FDR of 0.01. The minimum peptide length was seven amino acids. Results were matched between runs with a time window of 2 min for biological replicates. Peptide ion intensities produced by MaxQuant from the spatial references together with the time-series μ OR-APEX2 samples were summarized to protein intensities using the R package MSstats (v.3.23.1)¹³, specifically the function 'dataProcess' with default arguments except the outlier and noise filters³⁵ were enabled by setting 'remove_uninformative_feature_outliers=TRUE' and 'featureSubset='highQuality''. Log-transformed protein intensities were normalized per run using an equalize-medians procedure.

Digested PM-APEX2 samples, EYA4-APEX2 samples and μ OR-APEX2 samples derived from SH-SY5Y cells were analyzed on an Orbitrap Exploris 480 mass spectrometry system (Thermo Fisher Scientific) coupled to an Easy nLC 1200 nano-flow ultra-high-pressure liquid chromatography (Thermo Fisher Scientific) interfaced via a Nanospray Flex nanoelectrospray source. Samples were reconstituted in 1% formic acid and loaded onto a C18 column (25 cm \times 75 μ m ID packed with ReproSil-Pur-C18 AQ 1.9 μ m particles). Mobile phase A consisted of 0.1% FA, and mobile phase B consisted of 0.1% FA/80% ACN. Peptides were separated at a flow rate of 300 nl min⁻¹ using a gradient-increasing buffer B over 40 min to 16% B, followed by an increase over 26 min to 28% B and 4 min to 44% B. The mass spectrometer acquired data in a data-independent acquisition (DIA) mode, collecting one full scan in the Orbitrap at 120,000 resolution followed by DIA MS/MS scans within a m/z range of 350–1,050, with a fragmentation window size set to 20 m/z . The resolution of Orbitrap for MS/MS scans was set to 15,000 and a normalized collision energy of 30 was used for fragmentation. The DIA data were analyzed with Spectronaut (Biognosys) using direct DIA analysis default parameters for the identification and quantification of proteins. Normalization in Spectronaut was turned off. Data were searched against the SwissProt Human database (downloaded January 2017). Peptide ion intensities from Spectronaut were summarized to protein intensities using MSstats (v.3.22.1)¹³ implemented in the R package artMS (v.1.8.3) with default settings.

Statistical analysis of unbiased mass spectrometric data for APEX samples

μ OR-APEX2. Each protein's trend over the time course after treatment with agonists was scored by fitting the \log_2 (intensities) with continuous polynomial curves over time using the R functions 'lm' and 'poly'. To better fit the rapid changes, the collected time points were encoded by their ranks (1, 2, 3, 4, 5 and 6 for 0, 1, 5, 10, 30 and 60 min). All models included an additive term for the batch—a protein's background intensity was expected and allowed to vary between batches. Three time-dependent models were tested that varied in the maximum polynomial power that was allowed for the ranked-time model: linear, quadratic and cubic. The time-dependent models were compared with a null model that contained only the batch term using the R function 'anova' to compute an F -statistic and P value. The time model with the lowest P value was selected and the maximum model-predicted change between time 0 and a later time was used as the maximum \log_2FC for that protein. This process was repeated separately for the three agonists.

Spatial references. Proteins that varied between spatial references were scored with a single run of the MSstats function

'groupComparison' to compare between each nonredundant pair of spatial references. The input to MSstats was the entire set of spatial references with the μ OR-APEX2 data excluded. MSstats fits a single linear mixed model for each protein with a single categorical fixed-effect term for condition (spatial reference) and a random-effect term for batch. Using this model, MSstats reports pairwise differences in means as \log_2FC , and a pairwise P value calculated from a t -test assuming equal variance across all spatial references. A subset of 193 location-specific proteins was selected that could reliably distinguish locations by requiring P value < 0.005 and $\log_2FC > 1.0$ and observed intensity in all three replicates of at least one spatial reference greater than the 50th percentile of all observed protein intensities.

Spatial coefficients and spatial detrending of μ OR-APEX2 samples. For each μ OR-APEX2 sample, coefficients were calculated to estimate the contribution of each spatial reference to the observed protein intensity. First, protein intensities were scaled linearly between 0 and 1 by setting the maximum observed intensity (across all spatial reference and μ OR-APEX2 samples) for each protein to 1.0, and all other observations were set to the ratio of observed/maximum for that protein. Missing values were set to zero. A matrix representing protein intensities in the spatial references for all observed proteins, \mathbf{F} (3 spatial reference columns by 4,291 protein rows), was constructed using mean (per spatial reference) scaled intensity. The location-specific subset matrix (\mathbf{S}) was defined by using only the rows of \mathbf{F} that match the 193 location-specific proteins defined in the previous section. Location coefficients for each μ OR-APEX2 sample were then calculated using the nonnegative least-squares procedure in the R package nnls using the location-specific matrix \mathbf{S} and the vector of location-specific protein scaled intensities from each μ OR-APEX2 sample as inputs. We found this procedure would estimate low but nonzero coefficients where they were expected to be zero (for example, for lysosome at 0 min), probably due to fitting noise in the μ OR-APEX2 samples that the spatial references could not account for. To minimize these effects we used modified \mathbf{S} matrices that included three additional randomized columns, by sampling from \mathbf{S} . We repeated this randomization and nnls procedure 100 times and used the median value for the spatial reference coefficients. The three spatial reference coefficients for each μ OR-APEX2 sample were then combined into a matrix \mathbf{C} with 3 rows (spatial references) and 54 columns (μ OR-APEX2 samples; 3 ligands \times 6 time points \times 3 replicates). Estimates for sample-specific location components of all protein intensities were then predicted as the matrix product of $\mathbf{F} \times \mathbf{C}$. Location-detrended intensity values were then calculated by log-transforming both observed (\log_{Observed}) and predicted ($\log_{\text{Predicted}}$) intensity values and taking the difference, $\log_{\text{Observed}} - \log_{\text{Predicted}}$.

PM-APEX2. Changes in biotinylation of proteins at the plasma membrane in response to DAMGO and/or PTX were analyzed by fitting \log_2 (protein intensity) data using linear models with the R function 'lm'. The linear models included a term for time with DAMGO as a categorical variable, a term for \pm PTX and also the interaction term: DAMGO \times PTX, which measures the significance of the different response to DAMGO with, versus without, PTX.

EYA4-APEX2. Changes in biotinylation of proteins neighboring EYA4 in response to DAMGO and/or PTX were analyzed by the R package artMS (v.1.8.3), which makes use of the 'groupComparison' function with default settings implemented in MSstats (v.3.22.1)¹³.

GO enrichment method

Sets of proteins with significant changes were tested for enrichment of GO terms (GO biological process, molecular function and cellular component). The over-representation analysis was performed using the enricher function from R package clusterProfiler (v.3.99.0)³⁶. The GO terms and annotations were obtained from the R annotation package org.Hs.eg.db (v.3.12.0). To reduce the set of significantly enriched terms (at FDR < 0.01) to a set of nonredundant GO terms, we first constructed

a term tree based on distances (1 – Jaccard similarity coefficients of shared genes in GO) between all significant terms using the R function ‘hclust’. The term tree was cut at a specific level (R function cutree, $h = 0.99$) to identify clusters of nonredundant gene sets. For results with multiple significant terms belonging to the same cluster, we selected the most significant term (that is, lowest adjusted P value).

GSEA on changing locations of EYA4-APEX2

Significant cellular location changes between conditions were measured using GSEA as implemented in the R package *fgsea* (v.1.17)³⁷. Changes in protein intensity were scored using \log_2FC comparing samples and without DAMGO. Proteins were assigned to locations according to their ‘NMF Localization’ from Human Cell Map (v.1) downloaded on 7 June 2021 (<https://humancellmap.org/resources/downloads/preys-latest.txt>). The function *fgsea* was used with default options, and the $\log_{10}(P$ value) with its sign changed to match direction of enrichment was used as the significance score.

Targeted mass spectrometry data acquisition for APEX samples

Selected reaction monitoring (SRM) assays were generated for selected interactors of μ OR as well as localization markers and ribosomal proteins as internal controls for normalization (Supplementary Table 7). SRM assay generation was performed using Skyline³⁸. For all targeted proteins, proteotypic peptides and optimal transitions for identification and quantification were selected on the basis of a spectral library generated from the shotgun MS experiments. The Skyline spectral library was used to extract optimal coordinates for the SRM assays, for example, peptide fragments and peptide retention times. For each protein 2–5 peptides were selected on the basis of intensity, peptide length as well as chromatographic performance. For each peptide the 3–6 best SRM transitions were selected based on intensity and peak shape.

Digested peptide mixtures were analyzed by LC–SRM on a Thermo Scientific TSQ Quantiva MS system equipped with a Proxeon Easy nLC 1200 ultra-high-pressure liquid chromatography and autosampler system. Samples were injected onto a C18 column (25 cm \times 75 μ m ID packed with ReproSil–Pur–C18 AQ1.9 μ m particles) in 0.1% formic acid and then separated with an 80-min gradient from 5% to 40% buffer B (90% ACN/10% water/0.1% formic acid) at a flow rate of 300 nl min^{–1}. SRM acquisition was performed operating Q1 and Q3 at 0.7 unit mass resolution. For each peptide the best four transitions were monitored in a scheduled fashion with a retention time window of 4 min and a cycle time fixed to 2 s. Argon was used as the collision gas at a nominal pressure of 1.5 mTorr. Collision energies were calculated by $CE = 0.0348 \times (m/z) + 0.4551$ and $CE = 0.0271 \times (m/z) + 1.5910$ (CE, collision energy; m/z , mass to charge ratio) for doubly and triply charged precursor ions, respectively. RF lens voltages were calculated by $RF = 0.1088 \times (m/z) + 21.029$ and $RF = 0.1157 \times (m/z) + 0.1157$ (RF, RF lens voltage) for doubly and triply charged precursor ions, respectively. The resulting data were analyzed with Skyline for identification and quantification of peptides³⁸. MSstats (v.3.10.6) was used for statistical analysis¹³. Normalization across samples was conducted based on selected global standard proteins (RPL18A, RPL22, RPL28, RPL30, RPL35A, RPL6, RPL9, RPL9P7, RPL9P8, RPL9P9, RPS11). Model-based sample quantification implemented in MSstats was used to calculate the intensity of each protein in each biological sample and replicate combining all SRM transition intensities. The intensities for selected localization markers for the plasma membrane, early endosome and late endosome/lysosome were summed to calculate an intensity as a measure for receptor localization to each subcellular compartment.

EYA4 affinity purifications

For each affinity purification (EYA4 wild type (WT), EYA4 A633R mutant, EYA4 D375N, one GFP control, one empty vector control), HEK293 cells stably expressing μ OR (mouse) were plated per 15-cm dish and transfected with 10 μ g of individual Strep-tagged expression constructs

(2 μ g for GFP) after 20–24 hours. Total plasmid was normalized to 15 μ g with empty vector and complexed with PolyJet Transfection Reagent (SignaGen Laboratories) at a 1:3 μ g: μ l ratio of plasmid to transfection reagent based on manufacturer’s recommendations. After more than 38 hours, cells were dissociated at room temperature using Dulbecco’s phosphate buffered saline without calcium and magnesium (D-PBS) supplemented with 10 mM EDTA and subsequently washed with D-PBS. Each step was followed by centrifugation at 200g, 4 °C for 5 min. Cell pellets were frozen on dry ice and stored at –80 °C. For each bait and control, $n = 3$ independent biological replicates were prepared for affinity purification.

Frozen cell pellets were thawed on ice and suspended in 1 ml lysis buffer (IP buffer (50 mM Tris–HCl, pH 7.4 at 4 °C, 150 mM NaCl, 1 mM EDTA) supplemented with 0.5% Nonidet P40 substitute (NP40; Fluka Analytical) and cOmplete mini EDTA-free protease and PhosSTOP phosphatase inhibitor cocktails (Roche)). Samples were subjected to freeze–thaw cycle before incubation on a tube rotator for 30 min at 4 °C and centrifugation at 13,000g, 4 °C for 15 min to pellet debris. Affinity purifications were performed as follows. MagStrep ‘type3’ beads (30 μ l per sample; IBA Lifesciences) were equilibrated twice with wash buffer (IP buffer supplemented with 0.05% NP40) and incubated with the lysate on a tube rotator for 2 hours at 4 °C. Following incubation, beads were washed twice with wash buffer and with IP buffer. To directly digest bead-bound proteins, beads were resuspended in denaturation-reduction buffer (2 M urea, 50 mM Tris–HCl pH 8.0, 1 mM DTT). Bead-bound proteins were denatured and reduced at 37 °C for 30 min and, after bringing them to room temperature, alkylated in the dark with 3 mM iodoacetamide for 45 min and quenched with 3 mM DTT for 10 min. Proteins were then incubated at 37 °C, initially for 4 hours with 1.5 μ l trypsin (0.5 μ g μ l^{–1}; Promega) and then for another 1–2 hours with 0.5 μ l additional trypsin. All steps were performed with constant shaking at 1,100 r.p.m. on a ThermoMixer C incubator. Resulting peptides were combined with 50 μ l 50 mM Tris–HCl, pH 8.0 used to rinse beads and acidified with trifluoroacetic acid (0.5% final, pH < 2.0). Acidified peptides were desalted for MS analysis using a BioPureSPE Mini 96-well plate (20 mg PROTO 300 C18; The Nest Group) according to standard protocols.

Samples were resuspended in 4% formic acid/2% acetonitrile solution and analyzed on an Q-Exactive Plus MS system (Thermo Fisher Scientific) equipped with an Easy nLC 1200 ultra-high-pressure liquid chromatography system (Thermo Fisher Scientific) interfaced via a Nanospray Flex nanoelectrospray source. Samples were loaded onto a 75 μ m ID C18 reverse phase column packed with 25 cm ReproSil–Pur 1.9 μ m, 120 Å particles (Dr. Maisch). Mobile phase A consisted of 0.1% FA, and mobile phase B consisted of 0.1% FA/80% ACN. Peptides were separated by an organic gradient ranging from 4.5% to 32% acetonitrile over 53 min, then held at 90% B for 9 min at a flow rate of 300 nl min^{–1} delivered by an Easy1200 nLC system (Thermo Fisher Scientific). All MS1 spectra were collected with Orbitrap detection at 70,000 resolution and a scan range from 300 to 1,500 m/z , while the 20 most abundant ions were fragmented by higher-energy collisional dissociation and detected at a resolution of 17,500 in the Orbitrap. All AP–MS data were searched against the SwissProt Human (downloaded January 2017) using the default settings for MaxQuant (v.1.6.3.3)³⁴. Detected peptides and proteins were filtered to 1% FDR in MaxQuant, and identified proteins were then subjected to protein–protein interaction scoring with both SAINTexpress (v.3.6.3)³⁹ and CompPASS⁴⁰. We applied a filtering strategy to determine the final list of reported interactors. All protein interactions that possess a CompPASS WD score percentile >0.95, a SAINTexpress BFDR ≤ 0.05 . CompPASS scoring was performed using a larger in-house database derived from 11 baits that were prepared and processed in an analogous manner to this AP–MS dataset. This was done to provide a more comprehensive collection of baits for comparison, to minimize the classification of nonspecifically binding background proteins as high-confidence interactors. To determine the

mutant-dependent changes in protein interactions of EYA4, protein abundances for mutant and wild-type AP-MS were compared using MSstats (v.3.14.1)¹³. The protein interaction network was visualized using Cytoscape (v.3.8.1)⁴¹.

Generation and characterization of CRISPR knockout cell lines for EYA4 and KCTD12

KCTD12 and EYA4 knockout cell lines were generated by electroporation of Cas9 ribonucleoprotein complexes (Cas9 RNPs) into HEK293 cells stably expressing the μ OR (mouse) followed by clonal selection and characterization of the knockout. Electroporation was performed using the SF Cell Line 4D-Nucleofector X Kit S (Lonza) and 4D-Nucleofector (Lonza). Recombinant *Streptococcus pyogenes* Cas9 protein used in this study contains two nuclear localization signal (NLS) peptides that facilitate transport across the nuclear membrane. The protein was obtained from the QB3 Macrolab, University of California, Berkeley. Purified Cas9 protein was stored in 20 mM HEPES at pH 7.5 plus 150 mM potassium chloride, 10% glycerol and 1 mM tris(2-carboxyethyl)phosphine (TCEP) at -80°C . Each CRISPR (crRNA) and the *trans*-activating crRNA (tracrRNA) was chemically synthesized (Dharmacon/Horizon) and suspended in 10 mM Tris-HCl pH 7.4 to generate 160 μM RNA stocks. To prepare Cas9 RNPs, crRNA and tracrRNA were first mixed 1:1 and incubated for 30 min at 37°C to generate 80 μM crRNA:tracrRNA duplexes. An equal volume of 40 μM *S. pyogenes* Cas9-NLS was slowly added to the crRNA:tracrRNA and incubated for 15 min at 37°C to generate 20 μM Cas9 RNPs.

crRNAs targeting EYA4 (5'-CCGTAAGTGGGCAAGCTGTA-3') and KCTD12 (5'-CGTGACCCGGCGCTGCACGG-3') were designed by Dharmacon. For each reaction, roughly 3×10^5 HEK293 cells were pelleted and suspended in 20 μl nucleofection buffer. A 4 μl 20 μM Cas9 RNP mix was added directly to these cells and the entire volume transferred to the bottom of the reaction cuvette. Cells were electroporated using program CM-130 on the Amaxa 4D-Nucleofector (Lonza). Then, 80 μl prewarmed complete DMEM was added to each well and the cells were allowed to recover for 5 min at 37°C , followed by dilution in complete DMEM media for limited dilution to generate clonal cell lines. Clonal cell lines were characterized by genomic sequencing to confirm gene editing of EYA4 and western blot analysis for KCTD12 (Cell Signaling, cat. no. 81935S, dilution 1:1,000) to assess reduction in protein expression. GAPDH (BioLegend, cat. no. 607904, dilution 1:5,000) was used as a loading control for the western blot analysis.

Generation of polyclonal knockout cells for HaloTag assay

Stable cell lines expressing HaloTag- μ OR (human) were generated using HEK293T landing pad cells. These cells contain a genetically integrated doxycycline-inducible promoter, followed by a BxB1 recombination site and split iCasp9. This cell line was a gift from D. Fowler's group (Univ. Washington)⁴². To generate HaloTag- μ OR cell lines, landing pad constructs containing the N-terminal HaloTag- μ OR-P2A-PuroR fusion downstream of a BxB1-compatible *attB* site were cotransfected (1:1) with a BxB1 expression construct (pCAG-NLS-Bxb1 (ref. 43)) into the HEK293T landing pad cells using Lipofectamine 3000 according to the manufacturer's instructions in a six-well dish. All cells were cultured in $1 \times$ DMEM, 10% dialyzed FBS, 1% sodium pyruvate and 1% penicillin/streptomycin (D10) and incubated at 37°C in a 5% CO_2 humidified incubator. At 48 h following transfection, expression of integrated genes or iCasp9 selection system was induced by the addition of doxycycline ($2 \mu\text{g} \mu\text{l}^{-1}$) to D10 media. At 48 h after induction with doxycycline, AP1903 was added (10 nM) to cause dimerization of Casp9. Successful BxB1 recombination shifts iCasp9 out of frame, so only nonrecombined cells will die from iCasp9-induced apoptosis following the addition of AP1903. After 48 h of AP1903-Casp9 selection, the media was changed back to D10 with doxycycline and cells were allowed to recover for 48 h. Cells were then frozen until use.

Polyclonal KO cells were generated by electroporation of Cas9 RNP complexes into HEK293T cells stably expressing HaloTag- μ OR (human).

Electroporation was performed using the SF Cell Line 4D-Nucleofector X Kit S (Lonza) and 4D-Nucleofector (Lonza). Cas9 RNPs were generated as described above and crRNAs targeting selected proteins and nontargeting controls were designed by Dharmacon/Horizon (Supplementary Table 8). For each reaction, roughly 2×10^5 HEK293 cells were pelleted and suspended in 20 μl nucleofection buffer. Then, a 4 μl 20 μM Cas9 RNP mix was added directly to these cells and the entire volume transferred to the bottom of the reaction cuvette. Cells were electroporated using program CM-130 on the Amaxa 4D-Nucleofector (Lonza). Then 80 μl prewarmed complete DMEM was added to each well and the cells were allowed to initially recover for 10 min at 37°C followed by diluting with DMEM media, plating into 24-well plates and further recovery for 3 d. KO for selected genes was confirmed by western blot analysis, for example for VPS35 (Abcam, cat. no. ab10099, dilution 1:100) to assess reduction in protein expression. GAPDH (BioLegend, cat. no. 607904, dilution 1:5,000) was used as a loading control for the western blot analysis.

HaloTag-based internalization assay

Following CRISPR-mediated KO of target genes, 20,000 cells stably expressing the HaloTag- μ OR were seeded into each well of a poly-D-lysine-coated 24-well plate in D10 media containing doxycycline ($2 \mu\text{g} \text{ml}^{-1}$). For each KO strain, there were two wells of cells plated. Following 36 h of doxycycline expression of HaloTag- μ OR, media was replaced with D10. For each KO line, 48 h after seeding, one well was treated with 10 μM DAMGO and the other was left untreated. Cells were incubated at $37^{\circ}\text{C}/5\% \text{CO}_2$ during treatment with DAMGO. Following DAMGO treatment, plates were transferred to 4°C for 10 min to halt receptor trafficking. Subsequently, all cells were treated with a HaloTag dye, JF635i, dissolved in D10 to a final concentration of 200 nM for 30 min at 4°C . JF635i is a cell-impermeable dye that conjugates to cell-surface-expressed receptors. The JF635i dye solution was aspirated, and cells were treated with a cell-permeable HaloTag dye, JF525 in D10 (no phenol red), and incubated at 4°C again for 30 min. The JF525 dye solution was then aspirated, and cells were washed twice with PBS. D10 (no phenol red) was then added, and cells were incubated for a further 30 min to facilitate the washout of excess dye. Finally, cells were washed $1 \times$ with PBS-EDTA, detached using TrypLE Express for 10 min at room temperature, and resuspended in PBS + 2.5% dialyzed FBS and kept on ice before flow analysis. Stained cells were analyzed via flow cytometry using an Attune NxT flow cytometer. A total of 50,000 cells were collected for each condition. Cells were gated on FSC-A/SSC-A to separate HEK293T whole cells, and then FSC-A/FSC-H to find singlets. Following this, signals for each fluorescent dye, JF635i (RL1-A) and JF525 (BL1-A), were analyzed as follows.

Surface signal-to-interior signal ratios were normalized by multiplication by a constant factor, so that the mean surface:interior ratio across all replicates and guides of the nontargeting control at time zero was equal to 1.0. Ratios above 1.0 thus have more surface signal than the NTC, and ratios below 1.0 have less surface. The following statistical procedure was then repeated three times on \log_2 -transformed normalized ratios to find significant differences between gene knockouts and the nontargeting control for three different scores: log-normalized surface:interior ratios at time 0, log-normalized ratios after 30 min with agonist and the difference between log-normalized ratios after 30 min with agonist versus no agonist (also known as $\log_2\text{FC}$). For the latter, the subtraction was performed on matched data points within batches. First, the data across the four different batches were summarized to a single mean value per guide by fitting a linear model (R function 'lm') with additive terms for batch and guide. Outliers were detected as data points with modeled residuals with absolute value greater than 3 s.d. estimated on the entire model. If any outliers were discarded, the procedure was repeated, including detecting and discarding new outliers. The function 'emmeans' in R package emmeans (v.1.7.3) was then used to get an average across replicates for each guide. The averages for the

different guides were treated as independent measurements and fit to a linear model (R function 'lm') with only the targeted gene as the single dependent variable, with contrast statistics (*t*-test) computed using 'emmeans' with each gene knockout compared against the single NTC. *P* values were calculated using two-tailed tests on the *t* statistics.

Live-cell imaging

HEK293 cells stably expressing CMV:PM-APEX2-GFP and CMV:Lyso-APEX2-GFP were seeded onto 35-mm glass-bottom (12-mm glass) imaging dishes coated with poly-L-lysine. The cells were allowed to grow for 24 hours before live-cell imaging. Before imaging the Lyso-APEX2 cells were labeled with 60 nM final LysoTracker Deep Red (Thermo Fisher, cat. no. L12492) for 45 min at 37 °C. After this labeling period the cells were washed twice with HEK293 growth media (DMEM + 10% FBS) and media was exchanged with nonphenol red containing DMEM supplemented with 10% FBS. Before imaging the PM-APEX2 cells were labeled with Cell Mask Deep Red (0.75× final, Thermo Fisher, cat. no. C10046) for 5 min at room temperature to reduce internalization. After this labeling period the cells were washed following the above protocol for the Lyso-APEX2 cells. Cells were imaged using a Nikon Spinning Disk with a ×100 objective (1.49 numerical aperture). A 488-nm laser line (525/38 EM filter) was used to visualize the GFP-tagged construct and a 640-nm laser line (700/75 EM filter) was used to visualize the location markers.

Fixed-cell imaging

HEK293 cells stably expressing CMV:PM-APEX2-GFP, CMV:Endo-APEX2 and CMV:Lyso-APEX2-GFP were seeded onto no. 1.5 thickness, 12-mm coverslips coated with poly-L-lysine. The cells were allowed to grow for 24 hours before performing the APEX2 proximity labeling reaction. The cells were preincubated with 500 μM biotin-tyramide for 30 min at 37 °C in DMEM + 10% FBS. Before use, H₂O₂ was diluted to 2 mM final in room-temperature DMEM + 10% FBS containing 20 mM HEPES. Addition of the H₂O₂-containing media occurred at room temperature and the reaction was allowed to proceed for 30 s. The reaction was then stopped on ice with a quenching buffer consisting of PBS containing 10 mM sodium ascorbate, 1 mM Trolox and 10 mM sodium azide. The cells were washed with this quenching buffer three times and then fixed with 4% formaldehyde for 20 min at room temperature. The cells were then washed with TBS and blocked with an imaging buffer containing 3% BSA and 0.1% Triton X-100 in PBS. After an hour-long blocking step the cells were labeled with an anti-APEX2 primary (1:750, Abcam, cat. no. ab222414), neutravidin-405 (1:500, cat. no. 22831) and the Endo-APEX2 cells were labeled with an anti-EEA1 primary (1:500, cat. no. 48453S). This labeling was allowed to occur overnight at 4 °C and the following day samples were washed three times with PBS and labeled with secondary antibodies (1:1,000) in the same imaging buffer. Samples were then washed three times with PBS and mounted onto glass slides using Prolong Diamond Mountant (Thermo Fisher, cat. no. P36961) to preserve the GFP channel for validation of the APEX2 localization. Coverslips were allowed to fix overnight and samples were imaged on a Zeiss LSM 900 with Airyscan 2, following airyscan processing in Zen Blue software (Zeiss) and images were processed in FIJI.

Flow cytometric analysis of receptor trafficking

Flow cytometric analysis of receptor surface immunofluorescence was used to determine agonist-induced internalization and subsequent agonist-withdrawn surface recovery (recycling). HEK293 cells stably expressing FLAG-tagged μOR were left untreated as a control, incubated with 10 μM DAMGO for the noted time (0–30 min). To measure recycling, cells were incubated with 10 μM DAMGO for 30 min, washed and then incubated for an additional 30 min with 10 μM naloxone. All cells were washed twice in ice-cold PBS to stop trafficking, and incubated at 4 °C for 45 min with 2 μg ml⁻¹ Alexa647 (Life Technologies)-conjugated M1 anti-FLAG (Sigma, clone M1, cat. no.

F-3040, 1:1,000 dilution). Cells were washed once in PBS at 4 °C, and then mechanically lifted in PBS for an additional 45 min at 4 °C. Median fluorescence intensity of 10,000 cells per condition was measured using a FACSCalibur instrument (Becton Dickinson). Internalization was calculated as a fraction of the agonist-treated condition divided by untreated. Recycling was calculated as a fraction of surface-recovered receptor divided by the internalized receptor. At least four independent biological experiments were performed in triplicate for each condition.

Live-cell cAMP accumulation assay

HEK293 cells stably expressing μOR or μOR-APEX2 were transiently transfected with the cAMP biosensor pGLO-20F (Promega). Before agonist stimulation, cells were incubated with 250 μg ml⁻¹ luciferin for 45 min in DMEM without phenol red or serum. Then, 10 μM DAMGO and 10 nM isoproterenol, or 10 nM isoproterenol (reference condition), were added to each well and placed at 37 °C. Luminescence was recorded every 10 s with a CCD sensor for 20 min. Luminescence signal-generated agonist stimulation was integrated across 1 min of maximum average signal for the given condition, and normalized to the integrated signal from 1 min of the control condition.

cADDis cAMP biosensor assay

Real-time cAMP dynamics were measured using the Green Up cAD-Dis cAMP biosensor (Montana Molecular) according to the manufacturer's protocol. Briefly, HEK293 cell lines were lifted using TrypLE Express (Thermo Fisher) and resuspended in media supplemented with the appropriate volume of cADDis BacMam. Cells were plated into a 96-well plate (Corning, cat. no. 3340) at a concentration of 50,000 cells per well. After resting at room temperature for 30 min, plates were incubated under normal culture conditions overnight. Plates were washed twice with assay buffer (20 mM HEPES pH 7.4, 135 mM NaCl, 5 mM KCl, 0.4 mM MgCl₂, 1.8 mM CaCl₂, 5 mM D-glucose) before a 10-min incubation in a plate reader (Synergy H4, BioTek) prewarmed to 37 °C. Fluorescence was detected using an excitation wavelength of 500 nm and an emission wavelength of 530 nm every 30 s. After a 5-min baseline reading, vehicle or agonist(s) (100 nM isoproterenol, 10 μM DAMGO and 1 μM SST) were added, and fluorescence was measured for 30 min. A baseline fluorescence (F_0) was calculated for each well by averaging its fluorescence over the 5-min baseline reading, and the fluorescence response at each time point was calculated as the change in fluorescence ($\Delta F = F - F_0$) normalized to the baseline (F_0). To calculate an integrated cAMP, data points after agonist addition were summed. Each biological replicate represents the average of at least two technical replicates.

Electrophysiology

Whole-cell patch clamp experiments were performed as previously described⁴⁴. Briefly, HEK293 μOR stable cells were transfected with 0.7 μg GIRK1-F137S⁴⁵ and 0.1 μg tdTomato (tdT) per well. HEK293 cells were transfected with GIRK1-F137S, 0.1 μg tdT, 0.35 μg μOR, with or without 0.7 μg GFP-KCTD12 per well. Experiments were performed at least 24 h after transfection in a high potassium extracellular solution composed of (in mM) 120 KCl, 25 NaCl, 10 HEPES, 2 CaCl₂ and 1 MgCl₂ (pH 7.4). Solutions were delivered to a recording chamber using a gravity-driven perfusion system with exchange times of ~1 s. Cells were voltage clamped at -60 mV using an Axopatch 200B amplifier (Molecular Devices). Patch pipettes with resistances of 3–7 MΩ were filled with an intracellular solution composed of (in mM): 140 KCl, 10 HEPES, 3 Na₂ATP, 0.2 Na₂GTP, 5 EGTA, 3 MgCl₂ (pH 7.4). Inward GIRK currents were induced with perfusion of 100 nM or 10 μM DAMGO. Desensitization of currents was measured over 60 s DAMGO application. Recordings were analyzed using Clampfit (Molecular Devices) and Prism (GraphPad). Desensitization of the DAMGO-induced currents was calculated as follows: 100 × (1 - (amplitude before DAMGO washout)/(peak amplitude following DAMGO application)). The tau

of desensitization was calculated from the peak amplitude to DAMGO washout, fit to a single exponential curve.

Reporting summary

Further information on research design is available in the Nature Portfolio Reporting Summary linked to this article.

Data availability

Shotgun proteomics data access: RAW data and database search results have been deposited to the ProteomeXchange Consortium via the PRIDE partner repository⁴⁶ with the dataset identifier [PXDO31415](https://doi.org/10.26434/chemrxiv-2024-11). Targeted proteomics data access: Raw data and SRM transition files can be accessed, queried and downloaded via Panorama⁴⁷ <https://panoramaweb.org/MOR-APEX.url>. Source data are provided with this paper.

References

- Cox, J. & Mann, M. MaxQuant enables high peptide identification rates, individualized p.p.b.-range mass accuracies and proteome-wide protein quantification. *Nat. Biotechnol.* **26**, 1367–1372 (2008).
- Tsai, T.-H. et al. Selection of features with consistent profiles improves relative protein quantification in mass spectrometry experiments. *Mol. Cell. Proteomics* **19**, 944–959 (2020).
- Yu, G., Wang, L.-G., Han, Y. & He, Q.-Y. clusterProfiler: an R package for comparing biological themes among gene clusters. *OMICS* **16**, 284–287 (2012).
- Korotkevich, G. et al. Fast gene set enrichment analysis. Preprint at *bioRxiv* <https://doi.org/10.1101/060012> (2016).
- MacLean, B. et al. Skyline: an open source document editor for creating and analyzing targeted proteomics experiments. *Bioinformatics* **26**, 966–968 (2010).
- Choi, H. et al. SAINT: probabilistic scoring of affinity purification-mass spectrometry data. *Nat. Methods* **8**, 70–73 (2011).
- Sowa, M. E., Bennett, E. J., Gygi, S. P. & Harper, J. W. Defining the human deubiquitinating enzyme interaction landscape. *Cell* **138**, 389–403 (2009).
- Shannon, P. et al. Cytoscape: a software environment for integrated models of biomolecular interaction networks. *Genome Res.* **13**, 2498–2504 (2003).
- Matreyek, K. A., Stephany, J. J., Chiasson, M. A., Hasle, N. & Fowler, D. M. An improved platform for functional assessment of large protein libraries in mammalian cells. *Nucleic Acids Res.* **48**, e1 (2020).
- Hermann, M. et al. Binary recombinase systems for high-resolution conditional mutagenesis. *Nucleic Acids Res.* **42**, 3894–3907 (2014).
- Abreu, N., Acosta-Ruiz, A., Xiang, G. & Levitz, J. Mechanisms of differential desensitization of metabotropic glutamate receptors. *Cell Rep.* **35**, 109050 (2021).
- Vivaudou, M. et al. Probing the G-protein regulation of GIRK1 and GIRK4, the two subunits of the K_{ACh} channel, using functional homomeric mutants. *J. Biol. Chem.* **272**, 31553–31560 (1997).
- Vizcaino, J. A. et al. 2016 update of the PRIDE database and its related tools. *Nucleic Acids Res.* **44**, 11033 (2016).
- Sharma, V. et al. Panorama: a targeted proteomics knowledge base. *J. Proteome Res.* **13**, 4205–4210 (2014).

Acknowledgements

This work was supported by funding from the Defense Advanced Research Projects Agency (DARPA) under the Cooperative Agreements HR0011-19-2-0020 (to B.K.S., N.J.K., M.V.Z. and R.H.) and HR0011-20-2-0029 (to N.J.K. and R.H.). The views, opinions and/or findings contained in this material are those of the authors and should not be interpreted as representing the official views or policies of the Department of Defense or the US Government. This work further

received funding from the NIH (R01DA056354 to R.H., W.C.-M., and M.V.Z.; P01HL146366 to N.J.K. and R.H.; 1U01MH115747 to N.J.K. and M.V.Z.; R35GM124731 to J.L.; R01DA010711, DA012864 and MH120212 to M.V.Z.) and an NSF Graduate Research Fellowship (to N.A.). B.T.L. was a recipient of a K99/ROO (DA043607). E.B. was initially supported by an NIH/NRSA Postdoctoral Fellowship (F32CA260118) and is currently supported by a K99 (K99GM151441). M.K.H. was supported by a training grant from NIH (5T32GM139786). A.G.-H. is funded by the Margarita Salas Fellowship from the Spanish Ministry of Universities. J.L. is also supported by the Rohr Family Research Scholar Award and the Irma T. Hirsch and Monique Weill-Caulier Award. The work was carried out in the Thermo Fisher Scientific Mass Spectrometry Facility for Disease Target Discovery at the J. David Gladstone Institutes and the UCSF Center for Advanced Technology. We thank Luke D. Lavis and Claire Deo (Janelia / HHMI) for critical advice and materials in supporting the development of the Janelia Fluor (JF) dye-based receptor trafficking assay. We thank K. Obner and M. Eckhardt for reading the manuscript and providing critical feedback and members of both the von Zastrow and Krogan laboratories for helpful advice and comments.

Author contributions

B.T.L., B.J.P., M.V.Z. and R.H. conceived and directed the study with input from B.K.S. and N.J.K. B.T.L., Q.L. and P.K. performed APEX proximity labeling. B.J.P. developed the data analysis workflow and performed APEX data analysis with input from R.H. M.K.H., W.C.-M. and R.H. performed HaloTag-based trafficking assay with input from E.E.B. and M.V.Z. Electrophysiology experiments were performed by N.A., A.J.G.-H. and J.L. Constructs were cloned by B.T.L., J.X. and P.K. AP-MS experiments were performed by J.X. with input from R.H. AP-MS data analysis was conducted by Z.Z.C.N. with input from R.H. J.X. and R.H. generated and characterized knockout cell lines. E.E.B., B.T.L. and P.K. performed cAMP measurements with input from M.V.Z. B.N., B.T.L. and M.V.Z. performed imaging.

Competing interests

The Krogan laboratory has received research support from Vir Biotechnology, F. Hoffmann-La Roche and Rezo Therapeutics. N.J.K. has financially compensated consulting agreements with Maze Therapeutics and Interline Therapeutics. He is on the Board of Directors and is President of Rezo Therapeutics and is a shareholder in Tenaya Therapeutics, Maze Therapeutics, Rezo Therapeutics, GEn1E Lifesciences and Interline Therapeutics. B.K.S. is a founder of Epiodyne Inc., BlueDolphin LLC and Deep Apple Therapeutics, serves on the SAB of Schrodinger LLC and of Vilya Therapeutics, on the SRB of Genentech, and consults for Levator Therapeutics, Hyku Therapeutics and Great Point Ventures. The remaining authors declare no competing interests.

Additional information

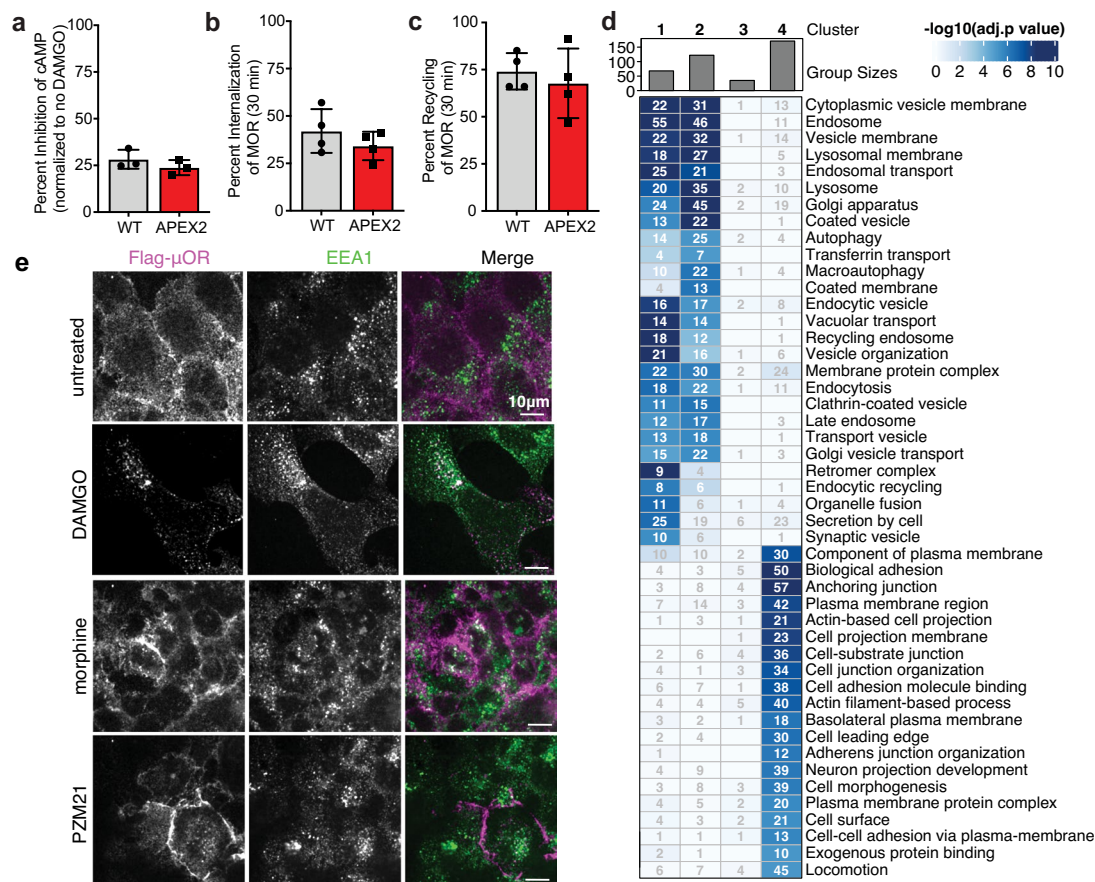
Extended data is available for this paper at <https://doi.org/10.1038/s41589-024-01588-3>.

Supplementary information The online version contains supplementary material available at <https://doi.org/10.1038/s41589-024-01588-3>.

Correspondence and requests for materials should be addressed to Mark Von Zastrow or Ruth Hüttenhain.

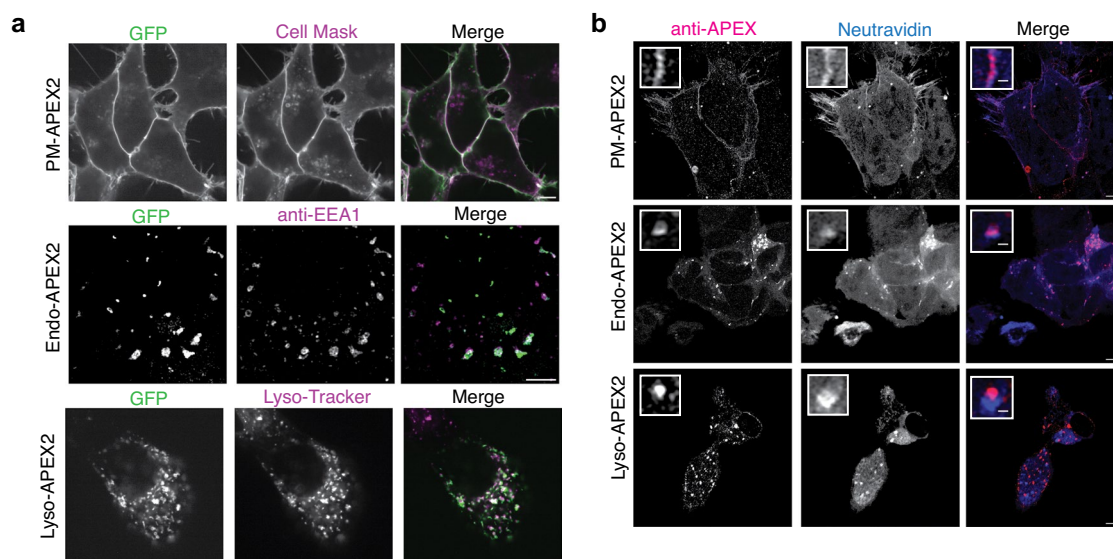
Peer review information *Nature Chemical Biology* thanks Nevin Lambert and the other, anonymous, reviewer(s) for their contribution to the peer review of this work.

Reprints and permissions information is available at www.nature.com/reprints.



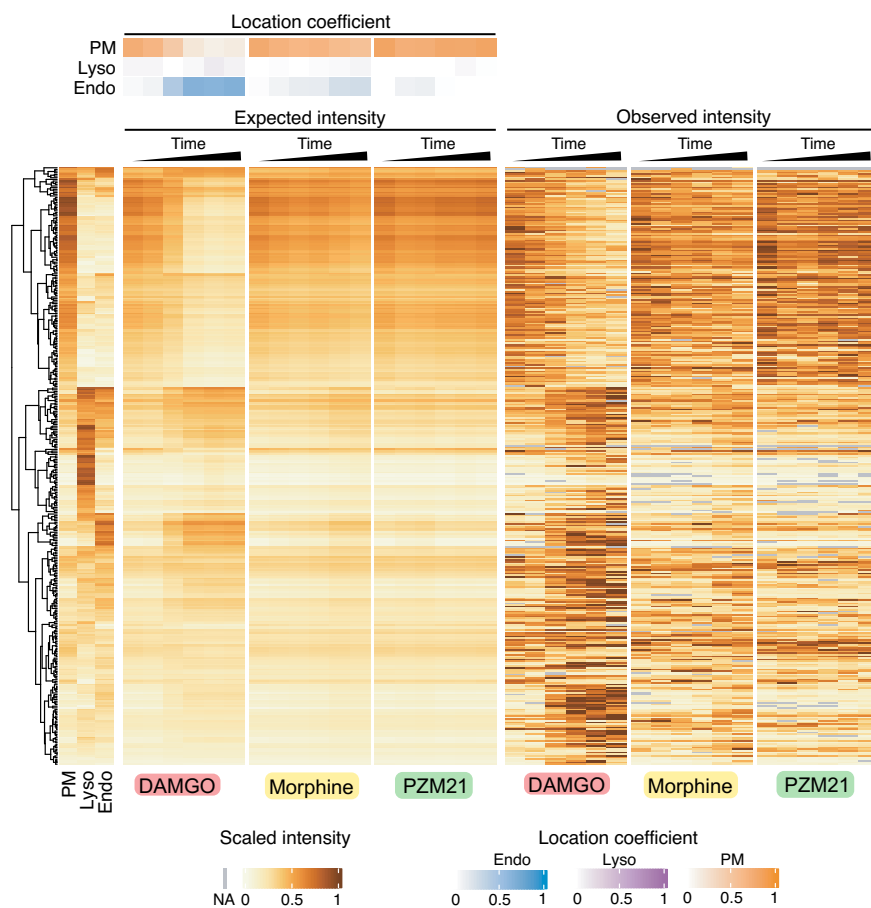
Extended Data Fig. 1 | APEX2-tagged μ OR remains functional and ligand-dependent proximal interaction networks of μ OR are enriched for proteins indicating cellular location. **a.** Receptor signaling was measured using a commercial cAMP biosensor (pGloSensor-20F). cAMP accumulation was measured after ~10 minutes of DAMGO/isoproterenol incubation and normalized to isoproterenol alone. Data from three independent experiments are presented as mean \pm SEM. **b.** Comparison of agonist-stimulated receptor internalization as assayed by loss of cell surface immunoreactivity and measured by flow cytometry comparing untreated (control) and treated samples (10 μ M DAMGO, 30 min). Data from four independent experiments are presented as mean \pm SEM. **c.** Comparison of cell surface recovery of receptors ('recycling') following 30 min of DAMGO application (10 μ M), agonist removal, and a 30 min recovery period in

the presence of antagonist (10 μ M). Data from four independent experiments are presented as mean \pm SEM. **d.** The heatmap shows all significantly enriched gene ontology terms (adjusted *P* value < 0.05) among the proteins that significantly change in the proximal protein environment of the μ OR upon activation with DAMGO, morphine, or PZM21 including the number of proteins that match the gene ontology terms. Cluster 1-4 refer to the clustering of the heatmap in Fig. 1b. **e.** Colocalization of μ OR with endosomes to monitor receptor trafficking following activation. HEK293 cells stable expressing the μ OR with an N-terminal Flag-tag were activated with 10 μ M DAMGO, morphine, or PZM21 for 10 min. The receptor was imaged using anti-Flag. Endosomes were marked with anti-EEA1. *n* = 3 independent biological replicates, representative example shown, Scale bar is 10 μ m.



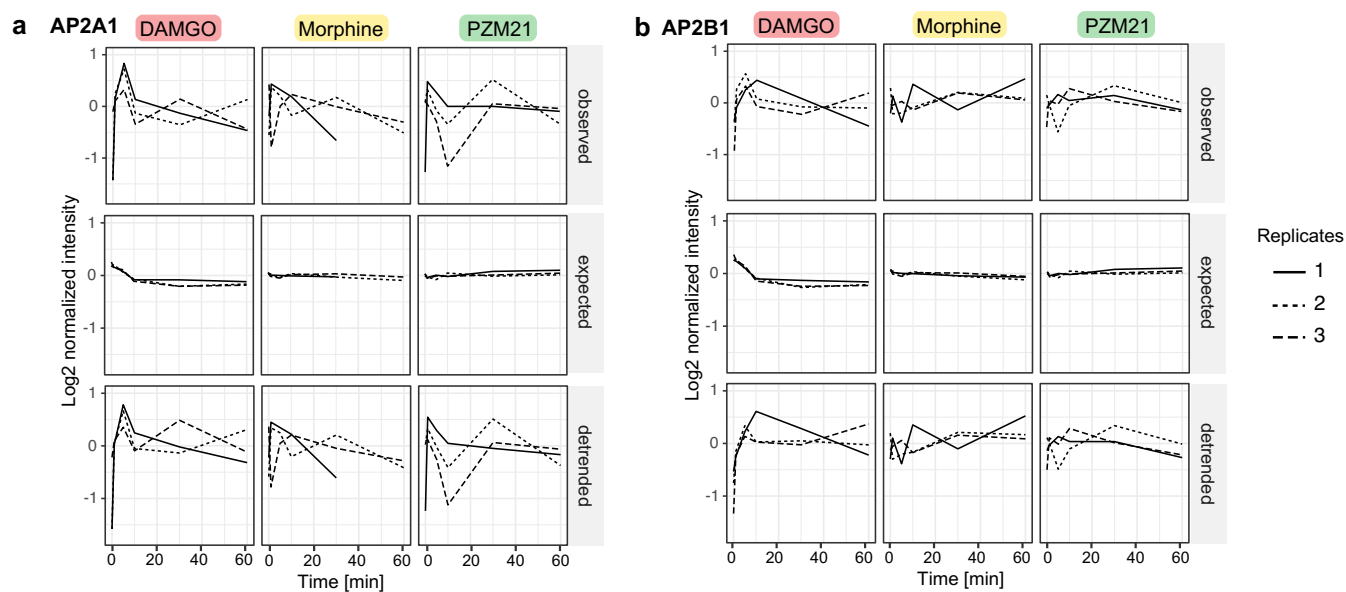
Extended Data Fig. 2 | Validation of spatial reference cell lines and μ OR trafficking. **a.** Colocalization of location markers with APEX2 spatial references. HEK293 cells stably expressing PM-APEX2, Endo-APEX2, or Lyso-APEX2 were imaged with either Cell Mask to mark the plasma membrane, anti-EEA1 to mark endosomes, or Lyso-Tracker to mark lysosomes. $n = 3$ independent biological

replicates, representative example shown, scale bar is $5\mu\text{m}$. **b.** Colocalization of biotin with APEX2 spatial reference constructs. Localization of biotin following APEX-mediated proximity labeling was probed with Neutravidin and APEX2 constructs were detected with anti-APEX. $n = 3$ independent biological replicates, representative example shown, scale bar is $5\mu\text{m}$.



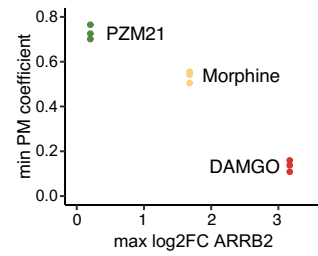
Extended Data Fig. 3 | Prediction of expected protein intensities based on location coefficients. The heatmap shows the location specific proteins that were selected by pairwise comparison of the spatial reference data and their scaled intensity measured across the spatial references (left side of the heatmap). Agonist and time point dependent expected protein intensities were estimated

by summing the spatial reference protein intensities that were weighted with their respective location coefficient. Observed protein intensities are shown as comparison (right side of the heatmap). Data from three independent experiments are presented as mean.

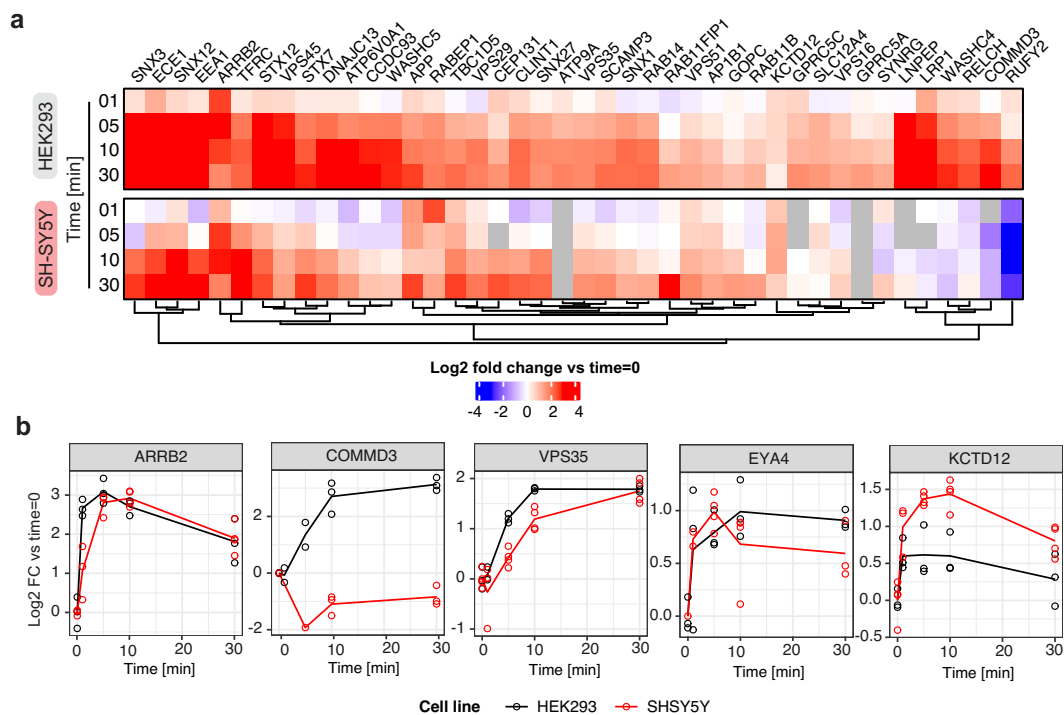
**Extended Data Fig. 4 | Effect of data detrending for AP2 complex subunits.**

Data detrending process to dissect localization specific effect from effect of interaction with the receptor for AP2A1 (a) and AP2B1 (b), members of the adaptor protein complex. Three different temporal profiles are depicted for

each protein, ligand, and replicate: the initial observed intensities, the expected intensities based on the location specific references, and the intensities after detrending. Data from three independent experiments are presented.

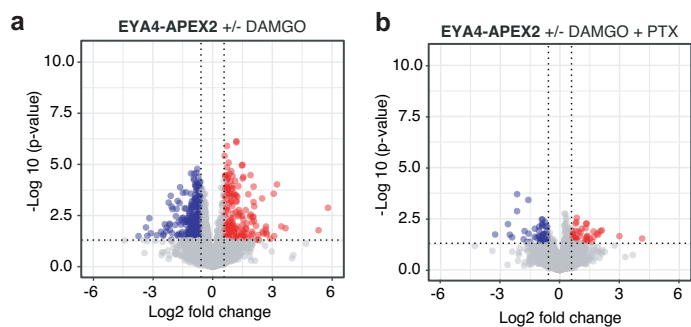


Extended Data Fig. 5 | Correlation between ARRB2 engagement upon μ OR activation with receptor trafficking. Correlation between the minimum location coefficient calculated for the plasma membrane (PM) and the maximum ARRB2 log2FC over the time course of μ OR activation with DAMGO (red), morphine (yellow) and PZM21 (green).



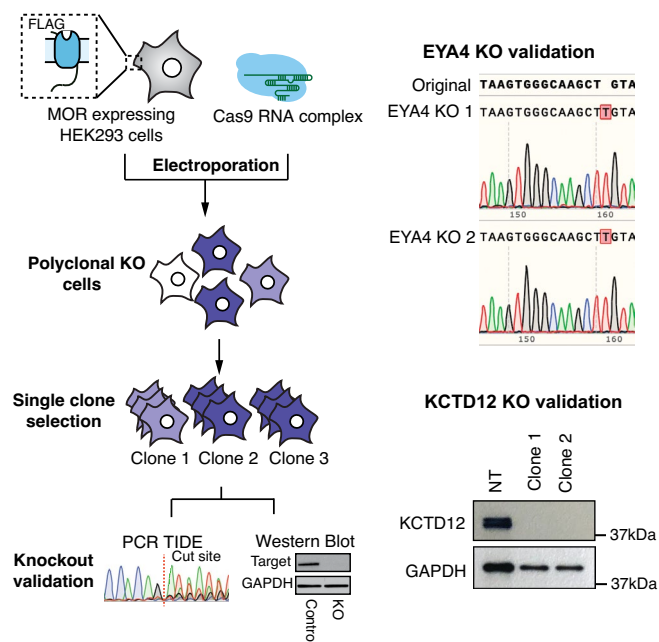
Extended Data Fig. 6 | Comparing the DAMGO-dependent proximal proteome changes of the μ OR in HEK293 and SH-SY5Y cells. **a.** Comparison of μ OR-APEX2 experiment upon activation with DAMGO in HEK293 and SH-SY5Y neuroblastoma cells. Heatmap focuses on all proteins significant for DAMGO in HEK293 data depicted in Fig. 3a. Data from three biological replicates are

presented as mean. **b.** Temporal profile for selected proximal interactors of the μ OR in HEK293 and SH-SY5Y cells. Line charts represent the log₂FC over the time course of receptor activation with DAMGO in HEK293 (black) and SH-SY5Y (red) cells. Data from three biological replicates are presented as mean.

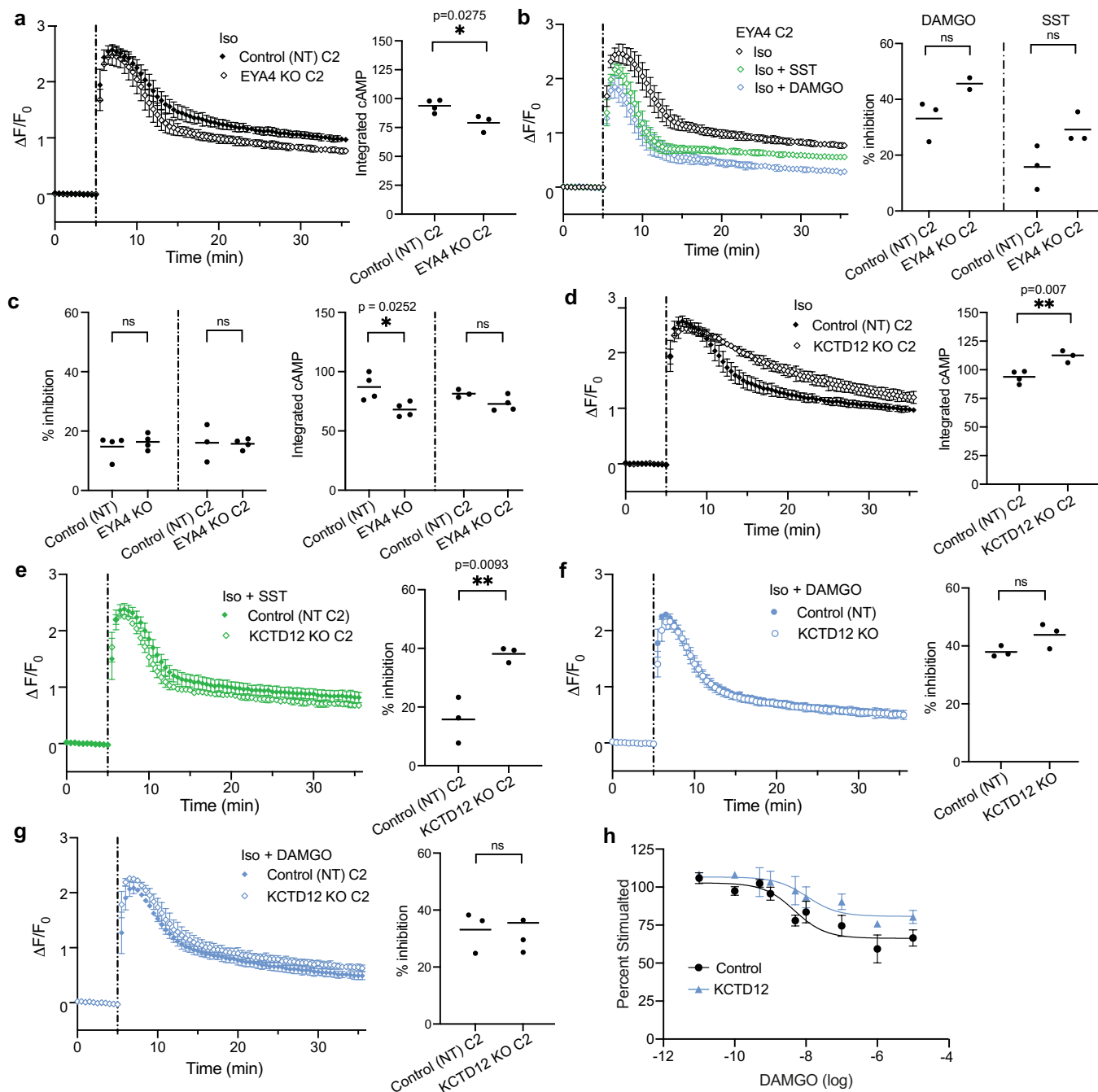


Extended Data Fig. 7 | Changes in proximity labeling of EYA4 upon μ OR activation. **a.** Volcano plot depicting $\log_{10} P$ value and $\log_2 FC$ comparing biotin labeled proteins in the proximity of EYA4 in the presence and absence of μ OR activation by treatment with 10 μ M DAMGO for 10 min. Data from three biological replicates are presented as mean. **b.** Volcano plot depicting $\log_{10} P$

value and $\log_2 FC$ comparing biotin labeled proteins in the proximity of EYA4 in the presence and absence of μ OR activation by treatment with 10 μ M DAMGO for 10 min and treatment with PTX. Data from three independent replicates are presented as mean.

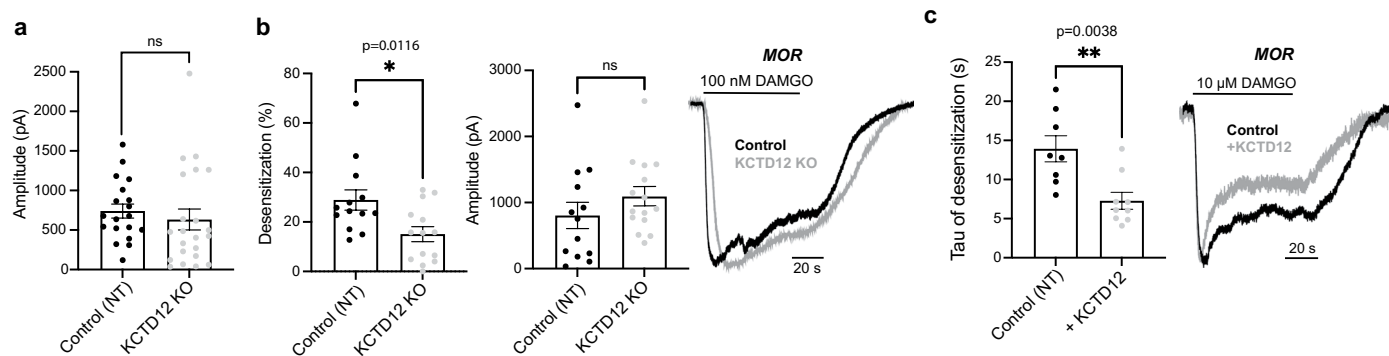


Extended Data Fig. 8 | Generation and validation of EYA4 and KCTD12 KO cell lines. KO was validated by PCR and sequencing (EYA4) or Western blot analysis (KCTD12). n = 2 independent biological replicates, representative examples shown.



Extended Data Fig. 9 | EYA4 and KCTD12 functional validation. **a.** cAMP activity in control non-targeting (NT) (closed) and EYA4 KO (open) HEK293 cells stably expressing the μ OR. Change in fluorescence intensity of cAMP biosensor upon stimulation with 100 nM isoproterenol (Iso) is plotted. $n = 3$, $*p = 0.0275$. **b.** cAMP activity EYA4 KO cells upon stimulation with Iso without (black) and with co-application of 1 μ M somatostatin (SST, green) or 10 μ M DAMGO (blue) is plotted. Iso curve is repeated from panel A. $n = 3$. **c.** Percent inhibition of Iso-stimulated cAMP with co-application of DAMGO (left) and integrated Iso-stimulated cAMP (right) in control non-targeting (NT) and EYA4 KO cell lines stably expressing the μ OR pretreated with PTX. $n = 3$, $*p = 0.0252$. **d.** cAMP activity in control (closed) and KCTD12 KO (open) HEK293 cells stably expressing the μ OR upon stimulation with Iso. Control curve is repeated from

panel A. $n = 3$, $**p = 0.007$. **e.** cAMP activity in control and KCTD12 KO cells upon stimulation with Iso and SST. Percent inhibition data for control is repeated from panel B. $n = 3$, $**p = 0.0093$. **f.** cAMP activity in control and KCTD12 KO cells upon stimulation with Iso and DAMGO for clones used in main figure (circles) with the main text control curve repeated from Fig. 5a. $n = 3$. **g.** cAMP activity in control and KCTD12 KO cells upon stimulation with Iso and DAMGO for clones used in supplemental figures (diamonds). $n = 3$. **h.** cAMP activity in WT cells stably overexpressing μ OR-APEX2 and transiently overexpressing KCTD12 or an empty vector control upon stimulation with Iso and DAMGO. $n = 3$. For all panels, data represent biological replicates, shown as individual data points or mean \pm SD, and significance was determined by unpaired, two-tailed t-test.



Extended Data Fig. 10 | Electrophysiology measurements for KCTD12 KO.

a. Summary bar graphs showing the average peak amplitudes of μ OR-mediated GIRK currents over 60 s 10 μ M DAMGO application, in control and KCTD12 KO HEK cells. Each point represents an individual cell. Error bars represent SEM.

b. Left, summary bar graphs showing the average peak amplitudes and percent desensitization of μ OR-mediated GIRK currents over 60 s 100 nM DAMGO, in control and KCTD12 KO HEK cells. Each point represents an individual cell. Unpaired, two-tailed t-test, * $p = 0.0116$. Error bars represent SEM. Right,

representative whole cell patch clamp recordings of μ OR-mediated GIRK currents in response to 60 s 100 nM DAMGO, in control and KCTD12 KO cells.

c. Left, Quantification of the tau of desensitization of μ OR-mediated GIRK currents over 60 s 10 μ M DAMGO application, without (control) and with KCTD12 overexpression in HEK 293 T cells. Each point represents an individual cell. Unpaired t-test, ** $p = 0.0038$. Error bars represent SEM. Right, representative whole cell patch clamp recordings showing GIRK currents mediated by μ OR activation over 60 s 10 μ M DAMGO.

Reporting Summary

Nature Portfolio wishes to improve the reproducibility of the work that we publish. This form provides structure for consistency and transparency in reporting. For further information on Nature Portfolio policies, see our [Editorial Policies](#) and the [Editorial Policy Checklist](#).

Statistics

For all statistical analyses, confirm that the following items are present in the figure legend, table legend, main text, or Methods section.

n/a | Confirmed

- The exact sample size (n) for each experimental group/condition, given as a discrete number and unit of measurement
- A statement on whether measurements were taken from distinct samples or whether the same sample was measured repeatedly
- The statistical test(s) used AND whether they are one- or two-sided
Only common tests should be described solely by name; describe more complex techniques in the Methods section.
- A description of all covariates tested
- A description of any assumptions or corrections, such as tests of normality and adjustment for multiple comparisons
- A full description of the statistical parameters including central tendency (e.g. means) or other basic estimates (e.g. regression coefficient) AND variation (e.g. standard deviation) or associated estimates of uncertainty (e.g. confidence intervals)
- For null hypothesis testing, the test statistic (e.g. F , t , r) with confidence intervals, effect sizes, degrees of freedom and P value noted
Give P values as exact values whenever suitable.
- For Bayesian analysis, information on the choice of priors and Markov chain Monte Carlo settings
- For hierarchical and complex designs, identification of the appropriate level for tests and full reporting of outcomes
- Estimates of effect sizes (e.g. Cohen's d , Pearson's r), indicating how they were calculated

Our web collection on [statistics for biologists](#) contains articles on many of the points above.

Software and code

Policy information about [availability of computer code](#)

Data collection

Data analysis

Unbiased mass spectrometry RAW data for APEX proximity labeling experiments were analyzed using the MaxQuant algorithm (version 1.5.5.1) for the identification and quantification of peptides and proteins (Cox and Mann, 2008). Peptide ion intensities produced by MaxQuant were summarized to protein intensities using the R package MSstats (version 3.23.1) (Choi et al., 2014). Targeted proteomics (Selected Reaction Monitoring, SRM) assay generation was performed using Skyline (MacLean, 2010). The resulting data was analyzed with Skyline (MacLean, 2010) for identification and quantification of peptides and MSstats (version 3.10.6) was used for statistical analysis (Choi et al., 2014). The over-representation analysis (ORA) for Gene Ontology terms was performed using the enricher function from R package clusterProfiler (version 3.99.0) (Yu et al, 2012). Cellular location changes were measured using gene set enrichment analysis as implemented in the R package fgsea (v 1.17) (Korotkevich, 2016). Data independent acquisition RAW mass spectrometry data were analyzed with Spectronaut (Biognosys) using direct DIA analysis default parameters for the identification and quantification of proteins. Peptide ion intensities from Spectronaut were summarized to protein intensities using MSstats (version 3.22.1) (Choi et al, 2014) implemented in the R package artMS (version 1.8.3) with default settings. Affinity purification mass spectrometry (AP-MS) RAW data for EYA4 were searched against the SwissProt Human (downloaded 01/2017) using the default settings for MaxQuant (version 1.6.3.3). Protein-protein interaction scoring for EYA4 was performed using with both SAINTexpress (version 3.6.3) (Choi et al., 2011) and CompPASS (version 1) (Sowa et al., 2009). Protein abundances for mutant and wildtype EYA4 AP-MS were compared using MSstats (version 3.14.1) (Choi et al., 2014). Protein interaction network was visualized using Cytoscape (version 3.8.1) (Shannon et al, 2003). Electrophysiology recordings were analyzed using Clampfit (Molecular Devices) and Prism (GraphPad).

For manuscripts utilizing custom algorithms or software that are central to the research but not yet described in published literature, software must be made available to editors and reviewers. We strongly encourage code deposition in a community repository (e.g. GitHub). See the Nature Portfolio [guidelines for submitting code & software](#) for further information.

Data

Policy information about [availability of data](#)

All manuscripts must include a [data availability statement](#). This statement should provide the following information, where applicable:

- Accession codes, unique identifiers, or web links for publicly available datasets
- A description of any restrictions on data availability
- For clinical datasets or third party data, please ensure that the statement adheres to our [policy](#)

Shotgun proteomics data access (Figure 1-3,5)

RAW data and database search results have been deposited to the ProteomeXchange Consortium via the PRIDE partner repository (Vizcaíno et al, 2016) with the dataset identifier PXD031415.

Reviewer account details:

Username: reviewer_pxd031415@ebi.ac.uk

Password: OvLPaURf

Targeted proteomics data access (Figure 1)

Raw data and SRM transition files can be accessed, queried, and downloaded via Panorama <https://panoramaweb.org/MOR-APEX.url> (Sharma et al, 2014).

Reviewer access:

Email: panorama+reviewer98@proteinms.net

Password: XStznYAS

Human research participants

Policy information about [studies involving human research participants and Sex and Gender in Research](#).

Reporting on sex and gender

Population characteristics

Recruitment

Ethics oversight

Note that full information on the approval of the study protocol must also be provided in the manuscript.

Field-specific reporting

Please select the one below that is the best fit for your research. If you are not sure, read the appropriate sections before making your selection.

Life sciences Behavioural & social sciences Ecological, evolutionary & environmental sciences

For a reference copy of the document with all sections, see nature.com/documents/nr-reporting-summary-flat.pdf

Life sciences study design

All studies must disclose on these points even when the disclosure is negative.

Sample size	No sample-size calculations were performed for this study. The number of required independent biological replicates that were performed was determined, as common in the field, by the requirement for statistical significance and reproducibility. It is an accepted practice in the field of proteomics, that biological triplicate measurements of APEX-MS and AP-MS samples are sufficient for measuring high confidence interactions using the methods and software performed in this study. This was also demonstrated in our previous study (Lobingier et al, Cell 2017). Three biological replicates were independently prepared for all proteomic datasets. All cAMP measurements were performed in at least biological triplicate measurements.
Data exclusions	No data were excluded from analyses.
Replication	All attempts at replication were successful. The number of biologically independent replicates are indicated in the figure legends.
Randomization	Sample randomization is not relevant to our study because experimental groups do not exist.
Blinding	Blinding is not relevant to the APEX-MS and AP-MS data because our data are acquired and processed systematically with established scoring algorithms, excluding human bias. Blinding was not performed for all other experiments, as knowledge about the treatment conditions was required for the researchers to be able to perform the experiments and ensure proper sample handling.

Reporting for specific materials, systems and methods

We require information from authors about some types of materials, experimental systems and methods used in many studies. Here, indicate whether each material, system or method listed is relevant to your study. If you are not sure if a list item applies to your research, read the appropriate section before selecting a response.

Materials & experimental systems

Methods

n/a	Involved in the study	n/a	Involved in the study
<input type="checkbox"/>	<input checked="" type="checkbox"/> Antibodies	<input checked="" type="checkbox"/>	<input type="checkbox"/> ChIP-seq
<input type="checkbox"/>	<input checked="" type="checkbox"/> Eukaryotic cell lines	<input checked="" type="checkbox"/>	<input type="checkbox"/> Flow cytometry
<input checked="" type="checkbox"/>	<input type="checkbox"/> Palaeontology and archaeology	<input checked="" type="checkbox"/>	<input type="checkbox"/> MRI-based neuroimaging
<input checked="" type="checkbox"/>	<input type="checkbox"/> Animals and other organisms		
<input checked="" type="checkbox"/>	<input type="checkbox"/> Clinical data		
<input checked="" type="checkbox"/>	<input type="checkbox"/> Dual use research of concern		

Antibodies

Antibodies used	<p>Primary antibodies: M1 anti-FLAG antibody (Sigma, Clone M1, Cat# F-3040, 1:1000 dilution for Flow cytometry), KCTD12 antibody (Cell Signaling, Cat# 81935S, dilution 1:1000 for Western Blot), GAPDH (BioLegend, Cat# 607904, dilution 1:5000 for Western Blot), VPS35 antibody (Abcam, Cat# ab10099, dilution 1:100 for Western blot), anti-APEX2 antibody (1:750, Cat#: ab222414), Neutravidin-405 (1:500, Cat#: 22831), anti-EEA1 antibody (Cell Signaling, Cat#: 48453S, 1:500).</p> <p>Secondary antibodies: Goat anti-rabbit 555 (Invitrogen, Cat# A21428, 1:10000), Goat anti-mouse 647 (Invitrogen, Cat# A21235, 1:10000), Goat Anti-Rabbit (Bio-Rad, Cat# 1706515, 1:10000), Donkey Anti-Goat (Abcam, Cat# ab6885, 1:10000)</p>
Validation	All antibodies were authenticated by the vendor. GAPDH antibody was validated to detect endogenous levels of GAPDH in cell lysates. KCTD12 and VPS35 antibodies were additionally validated by loss of detection after CRISPR/Cas9 knockout with multiple guide RNAs. M1 anti-FLAG antibody was also validated in cells that did not express a FLAG-tagged construct. anti-APEX2 antibody was validated in cells that did not express the APEX2-tagged construct. Neutravidin-405 antibody was validated in cells without proximity labeling.

Eukaryotic cell lines

Policy information about [cell lines and Sex and Gender in Research](#)

Cell line source(s)	HEK293 cells (CRL-1583, ATCC). SH-SY5Y cells (CRL-2266, ATCC). 293T (CRL-3216, ATCC). Information on the CRISPR knockout cell line generation can be found in the Methods section "Generation and characterization of CRISPR knockout cell lines for KCTD12 and EYA4".
Authentication	The cells were purchased and routinely maintained in our lab. They were not authenticated experimentally for these studies. For generated cell lines, expression of proteins of interest were validated by western blot.

Mycoplasma contamination

Cells used for APEX-MS and AP-MS were not tested for mycoplasma contamination.

Commonly misidentified lines
(See [ICLAC](#) register)

No commonly misidentified cell lines were used in this study.